Geochimica et Cosmochimica Acta xxx (xxxx) xxx

Contents lists available at ScienceDirect

Geochimica et Cosmochimica Acta

journal homepage: www.elsevier.com/locate/gca

# Metabolic imprints in the hydrogen isotopes of *Archaeoglobus fulgidus* tetraether lipids

Jeemin H. Rhim [a,*,1], Sebastian Kopf [b], Jamie McFarlin [b,c], Ashley E. Maloney [b], Harpreet Batther [b], Carolynn M. Harris [a], Alice Zhou [a,2], Xiahong Feng [a], Yuki Weber [d,3], Shelley Hoeft-McCann [d,4], Ann Pearson [d], William D. Leavitt [a,e]

[a] *Department of Earth Sciences, Dartmouth College, United States*
[b] *Department of Geological Sciences, University of Colorado Boulder, United States*
[c] *Department of Geology & Geophysics, University of Wyoming, United States*
[d] *Department of Earth & Planetary Sciences, Harvard University, United States*
[e] *Department of Chemistry, Dartmouth College, United States*

ARTICLE INFO

*Associate editor:* Magdalena Osburn

*Keywords:*
Archaeal lipids
Tetraether lipids
GDGTs
Biphytanes
Hydrogen isotope
Biomarkers

ABSTRACT

The stable hydrogen isotope composition of archaeal lipids is emerging as a potential paleoenvironmental proxy, adding to the well-established application of plant leaf wax-derived *n*-alkanes in paleohydrological reconstruction. A handful of studies reported relatively invariant and depleted hydrogen isotope compositions for archaeal lipids despite the range of different organisms and growth conditions explored. However, how modes of metabolism and physiological state (growth phase) affect the hydrogen isotope signatures of archaeal lipids remains poorly understood, limiting our ability to interpret archaeal lipid biomarker records from the environment. Here we conducted water isotope label experiments with a metabolically flexible and well-studied model archaeon *Archaeoglobus fulgidus* and quantified the hydrogen isotope fractionation between lipids and water in response to different carbon substrates and electron donor–acceptor pairs at different growth phases. The $^{2}H/^{1}H$ fractionation between lipids and water ($\varepsilon_{L/W}$) was overall negative. Both carbon metabolism and growth phase affected the magnitude of isotope fractionation in *A. fulgidus*; however, the changes in $\varepsilon_{L/W}$ values were relatively subtle where they ranged from –283 to –229 ‰ across all tested conditions, overlapping with the ranges observed for other archaea in previous studies. Isotope flux-balance model results suggest that $\geq$ 80 % and $\geq$ 50 % of lipid-bound H in *A. fulgidus* cultures directly reflect water isotope compositions (i.e., not via organic substrate or $H_2$) during autotrophy and heterotrophy, respectively. The model results also suggest two main mechanisms of consistent $^{2}H$ depletion observed in *A. fulgidus* tetraethers as well as other archaeal lipids reported in previous studies: 1) isotopic re-equilibration via upstream isomerization reactions involving $C_5$ units and 2) downstream double bond reduction catalyzed by a flavoenzyme geranylgeranyl reductase. These results are consistent with previous isotope flux-balance model results for a different archaeon. Finally, we synthesized available data to compare $\varepsilon_{L/W}$ patterns across all three domains of life: Eukarya, Archaea and Bacteria. Because they vary fundamentally in lipid biosynthesis pathways, we present comparative discussions in pairs, focusing on the shared biochemical mechanisms among isoprenoid lipids and potential signals of metabolic adaptations across prokaryotic lipids. Emerging patterns between diverse archaeal and eukaryotic isoprenoid lipids are consistent with the two proposed mechanisms for $^{2}H$ depletion identified (isomerization and final saturation). The patterns between archaeal isoprenoids and bacterial fatty acids suggest that the general state of energy limitation may also contribute to large, negative values of $\varepsilon_{L/W}$ observed in prokaryotic lipids. Altogether, these findings lend further support for the potential of archaeal lipid $\varepsilon_{L/W}$ as a paleohydrological proxy and provide a broader insight into the $^{2}H/^{1}H$ fractionation mechanisms potentially shared among prokaryotic and eukaryotic lipid biomarkers.

* Corresponding author.
*E-mail address:* jrhim@ucsb.edu (J.H. Rhim).
[1] Current address: University of California Santa Barbara, Santa Barbara, CA, USA.
[2] Current address: University of Michigan, Ann Arbor, MI, USA.
[3] Current address: Chroma Medicine, Boston, MA, USA.
[4] Current address: Wellesley College, MA, USA.

https://doi.org/10.1016/j.gca.2024.09.032
Received 10 February 2024; Accepted 26 September 2024
Available online 29 September 2024

## 1. Introduction

Hydrogen (H) plays a crucial role in most metabolic processes and is incorporated into biological molecules, often with distinct isotope fractionation patterns. Consequently, the ratio of stable hydrogen isotopes ($^2H/^1H$) of certain biomolecules can be used to track the H isotope compositions of source water, or the operation of specific biosynthetic pathways (Estep and Hoering, 1980; Hayes, 2001; Sessions et al., 1999). Lipid-bound H in hydrocarbons may resist isotope exchange for millions of years (Andersen et al., 2001; Sessions et al., 2004). Thus, sedimentary records of lipid $\delta^2H$ can be applied to reconstruct past ecological or hydrological states (Sachse et al., 2012; Sessions, 2016; McFarlin et al., 2019). The $\delta^2H$ of lipids produced by photoautotrophic eukaryotes as well as chemoautotrophic and heterotrophic bacteria have been studied in detail for this reason (e.g., Sessions et al., 1999; Chikaraishi and Naraoka, 2003; Zhang and Sachs, 2007; Zhang et al., 2009; Sachse et al., 2012; Sachs, 2014; Dawson et al., 2015; Osburn et al., 2016; Leavitt et al., 2016; Wijker et al., 2019; McFarlin et al., 2019). In contrast, there are only a handful of studies on the H isotope compositions of archaeal lipids (Kaneko et al., 2011; Dirghangi and Pagani, 2013; Wu et al., 2020; Lengger et al., 2021; Leavitt et al., 2023). As a consequence, the factors controlling the lipid/water fractionation ($\varepsilon_{L/W}$), as well as the extent and limits of proxy applications remain poorly understood for archaeal lipids.

Previous studies have revealed clear patterns of hydrogen isotope composition among different classes of compounds. The two major families of lipids—acetogenic and isoprenoid—consist of acetate and isoprene monomeric units, respectively (Pearson, 2014). Isoprenoid lipids are further divided into two groups, depending on whether the isoprene ($C_5$) building blocks are synthesized via the mevalonic acid (MVA) pathway (Lynen et al., 1958; Bloch, 1959) or the methylerythritol phosphate (MEP) pathway (Rohmer et al., 1993). The three different biosynthetic pathways of eukaryotic lipids (acetogenic, MVA, and MEP) are associated with distinct ranges of $\varepsilon_{L/W}$. In general, isoprenoid lipids have more negative $\varepsilon_{L/W}$ compared to acetogenic lipids within organisms (Estep and Hoering, 1980; Sessions et al., 1999). Among plant isoprenoid lipids, plastidic isoprenoids synthesized via the MEP pathway (e.g., phytols) are more depleted in $^2H$ than the cytosolic counterparts synthesized via the MVA pathway (Chikaraishi et al., 2004, 2009; Sessions et al., 1999).

Besides the differences observed across lipid biosynthesis pathways, other environmental and biological factors that control the hydrogen isotope compositions of eukaryotic and bacterial lipids have been identified in various culture studies. For lipids produced by photoautotrophic eukaryotes (e.g., plants and algae), net biosynthetic fractionation is relatively invariant but can be altered by some environmental factors (e.g., temperature, salinity, irradiance) and some factors intrinsic to an organism (e.g. growth rate in response to different stimuli and underlying genetics) (Sachs, 2014; Van Der Meer et al., 2015; Sachs and Kawka, 2015; Sachs et al., 2016, 2017; Maloney et al., 2016; Ladd and Sachs, 2017; Wolfshorndl et al., 2019). In general, these are well studied in eukaryotes, and have been accounted for in hydroclimate proxy studies (Sachse et al., 2012; Sessions, 2016; McFarlin et al., 2019). Bacterial fatty acids show a significantly wide range in $\varepsilon_{L/W}$ depending on the central metabolism a given bacteria operates, ranging from –400 to –200 ‰ (exclusively negative values) for (an)aerobic chemoautotrophs to –154 to + 380 ‰ for aerobic heterotrophs (Sessions et al., 2002; Campbell et al., 2009; Zhang et al., 2009; Dawson et al., 2015; Osburn et al., 2016; Leavitt et al., 2016; Wijker et al., 2019). For lipids produced by aerobic heterotrophs, H fluxes through $NADP^+$-reducing and NADPH-balancing reactions provide a quantitative explanation for the full range of $\varepsilon_{L/W}$ values observed (Wijker et al., 2019). Bacterial lipids found in sediments, especially those produced by aerobic heterotrophs, may have more useful applications as proxies for microbial metabolism and ecology rather than past hydroclimate (Zhang et al., 2009; Wijker et al., 2019).

Less is known about what information archaeal $\varepsilon_{L/W}$ record. Archaeal membrane lipids are distinguished from those of bacteria and eukaryotes by their ether (rather than ester) linkages to the glycerol backbone; *sn*-2,3-glycerol (rather than *sn*-1,2-glycerol) stereochemistry; and isoprenoid (rather than fatty acid) hydrophobic chains (Jain et al., 2014). Studies to-date indicate that archaeal isoprenoid lipids are generally depleted in $^2H$ (Kaneko et al., 2011; Dirghangi and Pagani, 2013; Wu et al., 2020; Lengger et al., 2021; Leavitt et al., 2023), with $\varepsilon_{L/W}$ values similar to those observed in isoprenoid lipids produced by eukaryotic photoautotrophs. In one recent study, continuous cultures of the obligate autotroph *Nitrosopumilus maritimus* revealed that $\varepsilon_{L/W}$ remains nearly constant across a 3-fold range in growth rate (Leavitt et al., 2023). Other studies have reported similarly large, negative values of $\varepsilon_{L/W}$ for archaea grown under heterotrophic conditions (Kaneko et al., 2011; Dirghangi and Pagani, 2013; Wu et al., 2020; Lengger et al., 2021).

On one hand, the observed similarity between isoprenoid lipids produced by eukaryotes and some archaea are not surprising given the shared biosynthetic pathway; however, an important question remains open regarding other factors that may affect archaeal lipid $\varepsilon_{L/W}$. While isoprenoid lipids from archaea and fatty acids from bacteria are not directly comparable, metabolic and physiological factors that cause a huge variation in bacterial lipid $\varepsilon_{L/W}$ should be tested on archaeal lipid $\varepsilon_{L/W}$ because some of these prokaryotes share similarities in their metabolic and physiological adaptations. In particular, testing the effects of carbon metabolism and growth phase on $\varepsilon_{L/W}$ within a single organism is important, considering that both osmo-mixotrophy (using both autotrophic and heterotrophic carbon sources) and slow growth (equivalent to conditions during stationary phase) are widespread phenomena in nature. For bacterial fatty acids, changes in carbon metabolism resulted in significantly different $\varepsilon_{L/W}$ values within a single organism for some species (e.g., *Cupriavidus oxalaticus* and *Paracoccus denitrificans*; Zhang et al., 2009; Osburn et al., 2016), but not in other species (sulfate-reducing bacteria; Dawson et al., 2015; Osburn et al., 2016; Leavitt et al., 2016).

In this study, we conducted pure culture experiments to better understand factors influencing $\varepsilon_{L/W}$ in archaeal lipids. To test the effect of metabolism on $\varepsilon_{L/W}$ within a single organism, we cultivate a metabolically flexible archaeon *Archaeoglobus fulgidus* in batch cultures on different carbon substrates and electron donor–acceptor pairs (lactate-thiosulfate, lactate-sulfate, and $H_2/CO_2$-thiosulfate). We also probe the effect of growth phase by comparing biomass harvested at exponential and stationary growth phases and track the fraction of water incorporated into the final product lipid by using different water isotope compositions of growth media. We then interpret the regression parameters derived from water isotope label experiments with an isotope flux-balance model informed by the enzymatic steps involved in the Wood-Ljungdahl (reductive acetyl-CoA) pathway used by *A. fulgidus* as well as archaeal isoprenoid lipid biosynthesis pathways used by all tetraether-producing archaea. In addition to *A. fulgidus*, we examine two thermoacidophilic archaea (*Acidianus* sp. DS80 and *Metallosphaera sedula* DSM 5348 T) for additional $\varepsilon_{L/W}$ measurements. We synthesize our new findings in the domain Archaea along with other available archaeal lipid $\varepsilon_{L/W}$ data as well as representative $\varepsilon_{L/W}$ values from domains Bacteria and Eukarya, and highlight factors that underlie patterns in $\varepsilon_{L/W}$ across the three domains of life.

## 2. Materials and Methods

### 2.1. Culture Strains and Growth

*Archaeoglobus fulgidus* str. VC-16 (DSM4304) was obtained from Deutsche Sammlung von Mikroorganismen und Zellkulturen (Braunschweig, Germany) and grown in batch cultures on two different carbon substrates and electron acceptors (Table 1). Culture media was prepared following the DSMZ 399 recipe with modifications as follows

(per liter): 0.34 g KCl, 4.00 g $MgCl_2{\cdot}6\ H_2O$, 3.45 g $MgSO_4{\cdot}7\ H_2O$, 0.25 g $NH_4Cl$, 0.14 g $CaCl_2{\cdot}2\ H_2O$, 0.11 g $K_2HPO_4{\cdot}3\ H_2O$, 0.20 g $KH_2PO_4$, 18.00 g NaCl, 2.52 g $NaHCO_3$, 2 mL $Fe(NH_4)_2(SO_4)_2{\cdot}7\ H_2O$ (0.1 % w/v), and 10 mL trace elements (DSMZ 141). After autoclaving, sterile anoxic solutions were added to the medium to a final concentration of 3.2 mM L-cysteine-HCl and 1 % (v/v) vitamin solution (DSMZ 141). When thiosulfate was used as an electron acceptor, 4.00 g/L $MgCl_2{\cdot}6\ H_2O$ and 3.45 g/L $MgSO_4{\cdot}7\ H_2O$ were replaced with 4.70 g/L $MgCl_2{\cdot}6\ H_2O$ and 3.48 g/L $Na_2S_2O_3{\cdot}5\ H_2O$. For heterotrophic growth, lactate was used as an electron donor and carbon source, 20 mM of Na-lactate solution was added and incubated with approximately 1 bar of $N_2/CO_2$ (80:20, v/v) headspace; for autotrophic growth, lactate was omitted and $H_2$ and $CO_2$ were used as an electron donor and carbon source, respectively, with 21 psig $H_2/CO_2$ (80:20, v/v) in the headspace. The headspaces of autotrophic cultures were flushed and re-pressurized with $H_2/CO_2$ once per day after each OD measurement. The $\delta^2H$ of culture media was manipulated by volumetrically diluting 99.9 % purity $^2H_2O$. The measured values of $\delta^2H$ in the final culture media in control (uninoculated) bottles were: 371.5 ‰, 180.7 ‰ and –64.2 ‰ for the T-L condition; 369.3 ‰, 178.8 ‰ and –62.1 ‰ for the S-L condition; and 355.1 ‰, 169.3 ‰ and –67.2 ‰ for the T-$H_2/CO_2$ condition.

All cultures of *A. fulgidus* were incubated at 82 °C. Heterotrophic cultures were incubated statically, and autotrophic cultures were shaken at 200 rpm to increase gas exchange between the $H_2/CO_2$ headspace and culture media. The optical density at 600 nm ($OD_{600}$) of samples was used for monitoring growth, and linearity against direct cell counts was confirmed (depth 0.02 mm; Petroff-Hausser Counter 3900) throughout the absorbance range. Biomass samples were harvested twice per experiment, one during mid-exponential phase and the other during early stationary phase. To harvest, 50 mL of culture was centrifuged for 15 min at 4 °C and 4500 *g* and resulting wet cell pellets were stored at –80 °C until lipid extraction.

Batch cultures of *Acidianus* sp. DS80 and *M. sedula* DSM 5348 T were grown for additional archaeal lipid $\varepsilon_{L/W}$ measurements (not for water isotope labeling experiments or isotope flux-balance model). *Acidianus* sp. DS80 was grown as previously described in (Rhim, Zhou et al., 2024), and *M. sedula* was grown in Brock basal salts medium with Allen's trace element mixture (Brock et al., 1972). See Supplementary Material for additional details for growth conditions for *Acidianus* sp. DS80 and *M. sedula*.

### 2.2. Lipid Extraction, Ether Cleavage, and Quantification

Frozen cell pellets were lyophilized overnight, and dry cell pellets were extracted using acidic hydrolysis-methanolysis. Briefly, dry cell pellets were physically disrupted in 1.5-mL microcentrifuge tubes by vortexing with methanol (MeOH) and *ca*. 250 µL of 100 µm combusted glass beads for 10 min at 3000 rpm using a Disruptor Genie (Scientific 126 Industries, SI-DD38). After excess MeOH was evaporated, octacosanol ($C_{28}$) or lignocerol ($C_{24}$) and $C_{46}$ GTGT were added to all samples as internal extraction standards. Samples were incubated at 65 °C for 90 min with 3 N methanolic HCl (33 % water content) to hydrolyze tetraether headgroups. Methyl *tert*-butyl ether (MTBE) was added to the cooled samples at a ratio of 3:2 (acid:MTBE, v/v), and samples were sonicated for 5 min (Qsonica Q500, Newtown, CT, USA). After sonication, n-hexane was added at a 1:1 ratio (MTBE:hexane, v/v), vortexed, and centrifuged at 15,000 g for 3 min. The upper organic phase was collected three times with n-hexane for the two subsequent rounds. The resulting total lipid extracts (TLEs) were dried under $N_2$ and proceeded to ether cleavage or stored at –20 °C until ether cleavage.

**Table 1**
Summary of culture experiments.

| Experimental Condition | electron donor | electron acceptor | carbon source |
|---|---|---|---|
| Thiosulfate-Lactate (T-L) | Lactate (20 mM) | Thiosulfate (14 mM) | Lactate (20 mM) |
| Sulfate-Lactate (S-L) | Lactate (20 mM) | Sulfate (14 mM) | Lactate (20 mM) |
| Thiosulfate-$H_2/CO_2$ (T-$H_2/CO_2$) | $H_2$ (g)* (80 % v/v) | Thiosulfate (14 mM) | $CO_2$ (g)* (20 % v/v) |

* The headspace of autotrophic cultures was filled with 21 psig $H_2/CO_2$ (80:20, v/v) and re-pressurized with $H_2/CO_2$ once per day after each OD measurement.

Ether bonds were cleaved in 57 % hydroiodic acid (HI) at 125 °C for 4 h. Then the organic phase was collected three times using n-hexane. The resulting alkyl iodides were reduced to alkanes (biphytanes, BPs) with $H_2$ in the presence of $Pt^{(IV)}O_2$ (Kaneko et al., 2011). Hydrogenated samples were passed through combusted pasteur pipettes with glass wool plugs to remove $PtO_2$ powder. Filtered samples were dried under $N_2$ and stored at –20 °C until analysis. The resulting ether-cleaved BPs were analyzed on a single quadrupole gas chromatography-mass spectrometer (GC–MS; Thermo ISQ LT with TRACE 1310) for compound identification and on a GC-flame ionization detector (GC-FID; Thermo TRACE 1310) for quantification, both housed in the CU Boulder Earth Systems Stable Isotope Laboratory at the University of Colorado Boulder.

### 2.3. Hydrogen isotope analysis and data processing

The $\delta^2H$ of BPs was analyzed on a GC-pyrolysis-isotope ratio MS (GC-P-IRMS) on a GC IsoLink II IRMS System (Thermo Scientific) in the CU Boulder Earth Systems Stable Isotope Laboratory at the University of Colorado Boulder. The GC-P-IRMS system consists of a Trace 1310 GC fitted with a programmable temperature vaporization (PTV) injector and either a 30 m ZB5HT column (i.d. = 0.25 mm, 0.25 µm, Phenomenex, Torrance, CA, USA) or a 60 m DB1 column (i.d. = 0.25 mm, 0.25 µm, Agilent, Santa Clara, CA, USA), ConFlo IV interface, and MAT 253 Plus mass spectrometer (Thermo Scientific).

*A. fulgidus* has been observed to produce both tetraether and diether lipids, with the majority of GDGT with no ring (GDGT-0) and a small fraction with up to two pentacyclic rings (Lai et al., 2008). The tetraether-to-diether ratio for *A. fulgidus* is expected to be ~ 1:1 at the growth temperature in this study (82 °C; Lai et al., 2008), and we focus on the tetraether fraction for the rest of the discussion. In line with the previous observations, the majority of BPs derived from *A. fulgidus* GDGT did not have rings (BP-0). All $\delta^2H$ values reported in this study are for BP-0.

All hydrogen isotope ratios are reported in the standard delta notation ($\delta^2H$) in permil (‰) units, against the Vienna Standard Mean Ocean Water (VSMOW) international standard:

$$\delta^2H = \left[\frac{(^2H/^1H)_{sample}}{(^2H/^1H)_{VSMOW}} - 1\right] \times 1000 \quad (1)$$

The lipid-water hydrogen isotope fractionation factor is reported in alpha notation ($^2\alpha_{L/W}$), and fractionation is reported in epsilon notation ($^2\varepsilon_{L/W}$) in ‰:

$$^2\alpha_{L/W} = \frac{(^2H/^1H)_{lipid}}{(^2H/^1H)_{water}} \quad (2)$$

$$^2\varepsilon_{L/W} = \left[^2\alpha_{L/W} - 1\right] \times 1000 \quad (3)$$

Values of $\delta^2H$ were first determined relative to $H_2$ reference gas ($\delta^2H_{raw}$), and then calibrated externally using a standard *n*-alkane mixture (A6, containing $C_{15}$ through $C_{30}$ n-alkanes spanning –9 to –263 ‰ *vs*. VSMOW; A. Schimmelmann, Indiana University). The A6 standard was combined with a $C_{36}$ n-alkane ($nC_{36}$, –259.2 ‰ *vs*. VSMOW; A. Schimmelmann, Indiana University) and measured at regular intervals at different concentrations. The BP $\delta^2H$ calibration was done in R, using the packages *isoreader* (Kopf et al., 2021) and *isoprocessor* available at

github.com/isoverse. Details of the data reduction and calibration methods are described in (Leavitt et al., 2023). The RMSE of the calibration peaks was 4.2 ‰ (n = 613) across a peak size range from 6.2 to 59.9 Vs. The RMSE of the $C_{36}$ *n*-alkane internal standard was 7.5 ‰ (n = 90) across a peak size range from 6.4 to 50.9 Vs. Calibrated $\delta^2H$ values for the biphytanes were corrected for the H added during hydrogenation of alkyl iodides. The magnitude of isotope fractionation during hydrogenation was estimated by comparing the $\delta^2H$ values of two different alkyl standards measured under three conditions: 1) without any treatment; 2) after ether cleavage followed by hydrogenation using $H_2$ gas with two different isotopic compositions; and 3) after hydrogenation step only (to confirm negligible isotopic exchange with alkyl H's). The isotope fractionation associated with $PtO_2$-catalyzed hydrogenation calculated from the $\delta^2H$ measurements was –648 ± 137 ‰. This value was used to calculate final corrected $\delta^2H_{BP}$ values reported here. The hydrogenation correction ranged from 7.4 to 14.3 ‰ and increased analytical uncertainty by up to 1.2 ‰.

The $\delta^2H$ of the $H_2$ gas in the $H_2/CO_2$ headspace of autotrophic cultures was analyzed on a Thermo Gasbench II in the Stable Isotope Laboratory at Northwestern University. The $\delta^2H$ of non-exchangeable H in lactate used for heterotrophic cultures was calculated from the $\delta^2H$ values of phthalic acid-TMS and lactic acid-TMS measured on a GC-P-IRMS on a GC IsoLink II IRMS System (Thermo Scientific), in the CU Boulder Earth Systems Stable Isotope Laboratory at the University of Colorado Boulder, and the known $\delta^2H$ of non-exchangeable H in phthalic acid (A. Schimmelmann, Indiana University). The calculated final value for $\delta^2H$ of nonexchangeable H in lactate was –28.5 ± 21.1 ‰. Detailed method descriptions for derivatization, isotope analysis, and calculation for $\delta^2H$ of nonexchangeable H in lactic acid can be found in Supplementary Material.

The $\delta^2H$ of natural abundance and deuterium-enriched medium water was measured at the Stable Isotope Laboratory at Dartmouth College as previously described (Kopec et al., 2019). Briefly, water was reduced with chromium at 850 °C using the H-Device, and the $\delta^2H$ of the resulting gas was measured by an IRMS (Thermo Delta Plus XL). The measured $\delta^2H$ values were converted to the water $\delta^2H$ equivalent by calibrating with water standards with known isotopic compositions analyzed in the same way. For samples expected to be outside the range of the standards (e.g., the deuterium-enriched medium), samples were diluted with water standards. The 1σ uncertainty for $\delta^2H$ measurements is < 0.5 ‰.

### 2.4. Model implementation

An isotope flux-balance model was adapted from the conceptual framework described in Leavitt et al. (2023). Our model considers the Wood-Ljungdahl (reductive acetyl-CoA) pathway used by *A. fulgidus* for determining the sources and fluxes of H during acetyl-CoA (Ac-CoA) synthesis. It also considers the general archaeal lipid biosynthesis pathway for the accounting of total H budget in archaeal lipids. Analytical solutions for the model were calculated in R. Details of the model design and outcomes are described in section 4.

## 3. Results

### 3.1. Cultures and growth rates

*Archaeoglobus fulgidus* is a metabolically flexible strain from the phylum Euryarchaeota. We cultivated *A. fulgidus* in batch (closed-system) cultures on three different combinations of electron donors and acceptors (Table 1; Fig. 1A–C). In two treatments, *A. fulgidus* was grown as a heterotroph, using lactate as the carbon source and electron donor and sulfate or thiosulfate as the terminal electron acceptor. In the third treatment, *A. fulgidus* was grown as an autotroph, using $CO_2$ as the carbon source, $H_2$ as the electron donor, and thiosulfate as the terminal electron acceptor. Cultures were acclimated to each treatment by growing on respective substrate combinations for two or more passages before inoculation. Overall, heterotrophic conditions resulted in faster growth (T-L, $t_d$ = 6.2 ± 0.6 h; S-L, $t_d$ = 10.3 ± 1.7 h) compared to autotrophic growth (T-$H_2/CO_2$, $t_d$ = 19.3 ± 3.9 h) (Table 2; Fig. 1A–C).

### 3.2. Carbon metabolism and growth phase affect lipid $\delta^2H$ and regression parameters

Different modes of carbon metabolism and growth phase resulted in different isotope fractionation ($\varepsilon_{L/W}$) patterns observed in *A. fulgidus*. Comparing across cultures grown in unlabeled media, the two heterotrophic conditions resulted in similar $\varepsilon_{L/W}$ values (–229 ‰ for T-L and –246 ‰ for S-L during exponential phase; –239 ‰ for T-L and –243 ‰ for S-L during stationary phase; Table 2). The autotrophic condition and stationary growth phase resulted in overall larger fractionation (–255 ‰ during exponential phase; –283 ‰ during stationary phase for T-$H_2/CO_2$; Table 2).

Comparing across cultures grown in media with different water $\delta^2H$ values can be informed by the following isotopic mass balance as previously described (Zhang et al., 2009):

$$R_{BP} = f_W \cdot {}^2\alpha_{L/W} \cdot R_W + f_S \cdot {}^2\alpha_{L/S} \cdot R_S \quad (4)$$

where $R_{BP}$, $R_W$, and $R_S$ represent the $^2H/^1H$ ratios of BPs from GDGT-0 (BP-0), media water, and substrate (lactate for the heterotrophic conditions; $H_2$ for the autotrophic condition), respectively. $f_W$ and $f_S$ are the fractions of lipid-bound H originating from water and substrate, respectively. $^2\alpha$ represents the net isotope fractionation factor between lipid and water ($^2\alpha_{L/W}$) and between lipid and substrate ($^2\alpha_{L/S}$), respectively. In parallel cultures where only one parameter ($R_W$) is varied experimentally, measurements of $R_L$, $R_W$, and $R_S$ provide the basis for regression of $R_L$ on $R_W$.

Overall, the $\delta^2H_L$ values were strongly correlated with $\delta^2H_W$ values in all experiments (Table 2; $R^2 \geq 0.993$ and $p \leq 0.05$ in every regression). The regression slopes varied as a function of carbon metabolism and growth phase. The two heterotrophic conditions (T-L and S-L) and exponential growth phase resulted in lower slopes compared to the autotrophic condition (T-$H_2/CO_2$) and stationary growth phase. Slopes for the two heterotrophic conditions were similar (0.481 ± 0.017 for T-L, 0.477 ± 0.028 for S-L during exponential phase; 0.548 ± 0.015 for T-L, 0.519 ± 0.016 for S-L during stationary phase; Table 2). The autotrophic condition resulted in higher slopes (0.552 ± 0.019, exponential phase; 0.628 ± 0.025, stationary phase; Table 2). Notably, the higher slope observed during the stationary phase of the autotrophic culture was the closest to the slope estimated assuming $f_W$=1 (0.707) (Table 2; Fig. 1D).

## 4. *A. fulgidus* H-isotope flux-balance model

To further interpret these findings, we modified the isotope flux-balance model recently developed for an ammonia-oxidizing archaeon *N. maritimus* SCM1 (Leavitt et al., 2023) to reflect the biochemistry underlying the different modes of carbon metabolism in *Archaeoglobus fulgidus* VC-16. The overall conceptual framework consists of two parts for the stoichiometric accounting of: 1) methyl-H in Ac-CoA and 2) the 80 H atoms in the $C_{40}$ alkyl chain of BPs inherited from Ac-CoA. The former requires metabolism-specific information considering the mode (s) of carbon fixation and experimental conditions such as substrate availability, while the latter is informed by more universal information about archaeal isoprenoid biosynthesis. Below, we describe the details of the two parts of our model.

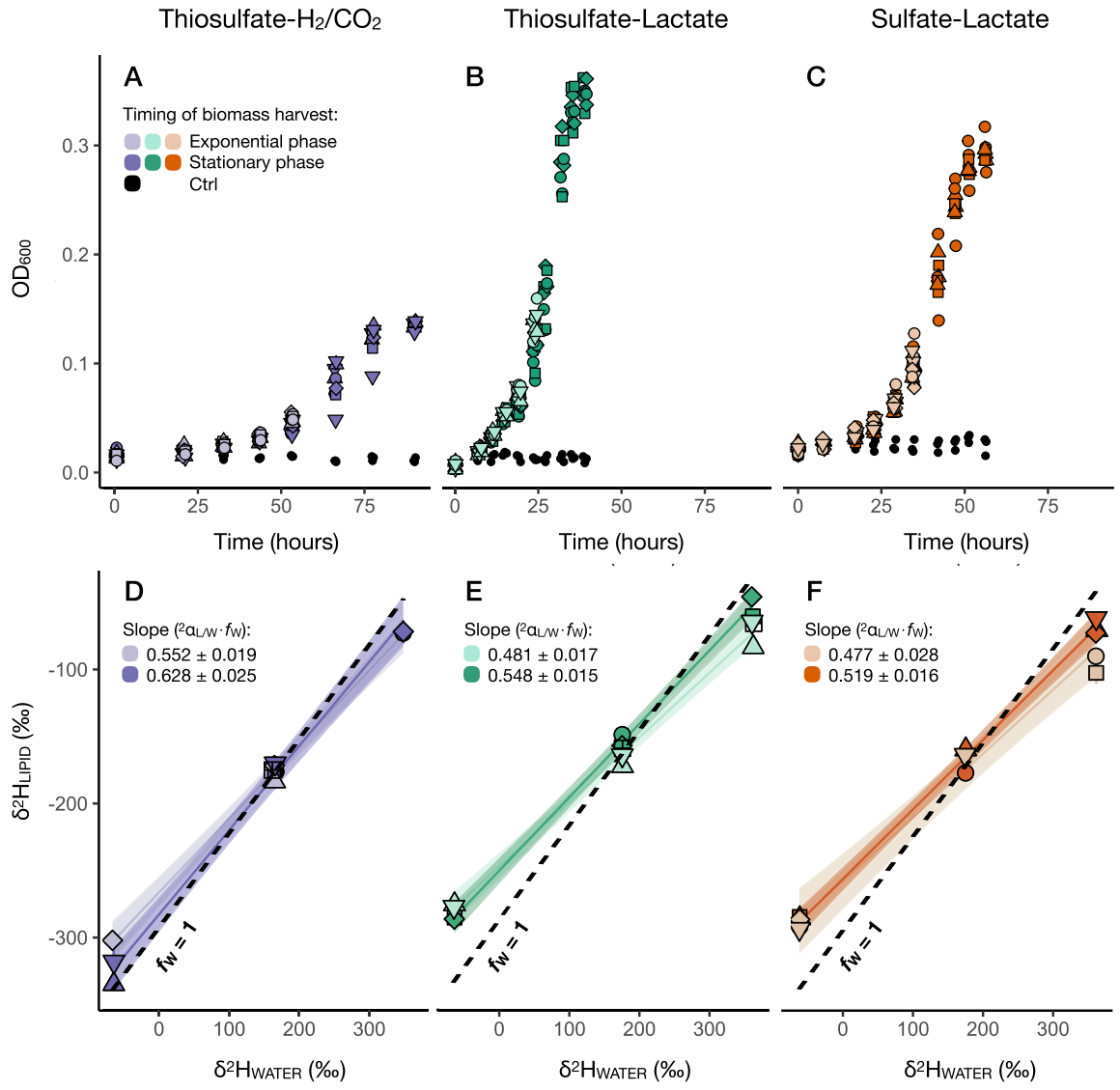


**Fig. 1.** Growth curves and regression of lipid $\delta^2H$ versus water $\delta^2H$ for *Archaeoglobus fulgidus*. Growth curves of *A. fulgidus* grown autotrophically on (A) thiosulfate and $H_2/CO_2$ or heterotrophically on (B) thiosulfate and lactate or (C) sulfate and lactate. Lighter color symbols represent triplicate cultures that were harvested for biomass during mid-exponential phase; darker color symbols represent triplicate cultures that were harvested for biomass during early stationary phase. Regression of biphytane hydrogen isotopic composition ($\delta^2H_L$) on water isotopic composition ($\delta^2H_W$) grown on (D) thiosulfate and $H_2/CO_2$, (E) thiosulfate and lactate, and (F) sulfate and lactate. Best-fit regression lines are shown in solid lines, with slope estimates in the legend. The dashed line represents the theoretical slope of 0.707 when $f_W$=1. See Table 2 for more details on regression parameters.

### 4.1. *Sources of lipid-H via the modified Wood-Ljungdahl pathway*

#### 4.1.1. *Heterotrophy*

*A. fulgidus* can grow autotrophically or heterotrophically via the modified reductive Ac-CoA or Wood-Ljungdahl pathway (Möller-Zinkhan et al., 1989; Möller-Zinkhan and Thauer, 1990; Hocking et al., 2014). During chemoorganoheterotrophic growth on lactate, the type species *A. fulgidus* VC16 couples the complete oxidation of organic substrates to $CO_2$ with the reduction of sulfate or thiosulfate to sulfide. In this study, the organic substrate was lactate. *A. fulgidus* oxidizes lactate via pyruvate and Ac-CoA using enzymes and cofactors involved in the $C_1$-pathway, similar to those found in methanogens, in reverse direction (Fig. 2A; Möller-Zinkhan et al., 1989; Möller-Zinkhan and Thauer, 1990). A D-lactate dehydrogenase in *A. fulgidus* catalyzes the first step of lactate oxidation to pyruvate coupled with the reduction of menaquinone (MQ), resulting in menaquinol ($MQH_2$) (Step 1, Fig. 2A; Kunow et al., 1993; Reed and Hartzell, 1999). The next step of pyruvate oxidation to Ac-CoA is catalyzed by pyruvate:ferredoxin oxidoreductase (Step 2, Fig. 2A; Kunow et al., 1993). The three H atoms in the methyl group of lactate most likely remain intact and are inherited to Ac-CoA. Some of these Ac-CoA products are used for biomass synthesis (Step 3.2, Fig. 2A), including isoprenoid lipid biosynthesis, while some of them are degraded further for the complete oxidation of lactate. For the latter, carbon monoxide dehydrogenase catalyzes both the reversible carbon–carbon cleavage of Ac-CoA and the oxidation of carbonyl group to $CO_2$ coupled with ferredoxin (Fd) reduction (Step 3.1, Fig. 2A; Möller-Zinkhan and Thauer, 1990).

The coenzymes involved in the downstream oxidative branch of Ac-CoA degradation could transfer hydrides (e.g., $F_{420}H_2$ in Steps 4 and 5, Fig. 2A). These fluxes of H are important to track because the hydrides from Ac-CoA (ultimately from lactate) can be recycled for NADP reduction, the product of which (NADPH) can donate hydrides to isoprenoid precursors during lipid biosynthesis. We assign $F_{420}$ and Fd as the electron acceptors for Steps 4–5 and Step 8, respectively (Fig. 2A), given that the genes relating to all steps of the reductive Ac-CoA pathway are expressed in *A. fulgidus* (Hocking et al., 2014) and

**Table 2**
Growth and isotope data for tetraether-derived biphytanes produced by *Archaeoglobus fulgidus* grown on different carbon substrates and electron donor–acceptor pairs.

| Substrate[a] | $t_d$ (h)[b] | Growth Phase[c] | Avg. OD[d] | $\delta^2H_W$[e] (‰) | s.d. (‰) | $\delta^2H_L$[f] (‰) | s.d. (‰) | $^2\varepsilon_{L/W}$ (‰) | s.d. (‰) | n[g] | Slope[h] ($^2\alpha_{L/W} \cdot f_W$) | s.e. | $R^2$ | *p* |
|---|---|---|---|---|---|---|---|---|---|---|---|---|---|---|
| T-L | 6.2 ± 0.6 | Exp | 0.147 | 362.4 | 0.2 | –73 | 6 | –320 | 3 | 3 | 0.481 | 0.017 | 0.996 | $1 \times 10^{-7}$ |
| | | | 0.135 | 176.0 | 0.2 | –167 | 7 | –292 | 3 | 3 | | | | |
| | | | 0.141 | –64.0 | 0.2 | –278 | 7 | –229 | 5 | 2 | | | | |
| | | Sta | 0.346 | 361.3 | 0.2 | –55 | 7 | –306 | 3 | 2 | 0.548 | 0.015 | 0.999 | $3 \times 10^{-6}$ |
| | | | 0.344 | 175.5 | 0.2 | –155 | 7 | –281 | 4 | 2 | | | | |
| | | | 0.351 | –63.7 | 0.2 | –288 | 9 | –239 | 6 | 2 | | | | |
| S-L | 10.3 ± 1.7 | Exp | 0.096 | 361.8 | 0.2 | –90 | 10 | –332 | 4 | 1 | 0.477 | 0.028 | 0.993 | $7 \times 10^{-5}$ |
| | | | 0.100 | 174.7 | 0.2 | –166 | 5 | –290 | 4 | 3 | | | | |
| | | | 0.082 | –61.7 | 0.2 | –292 | 6 | –246 | 4 | 2 | | | | |
| | | Sta | 0.307 | 361.4 | 0.2 | –70 | 6 | –317 | 3 | 2 | 0.519 | 0.016 | 0.998 | $4 \times 10^{-7}$ |
| | | | 0.295 | 175.4 | 0.2 | –171 | 5 | –294 | 3 | 2 | | | | |
| | | | 0.282 | –61.5 | 0.2 | –290 | 10 | –243 | 6 | 2 | | | | |
| T-$H_2$/$CO_2$ | 19.3 ± 3.9 | Exp | 0.052 | 348.3 | 0.2 | –75 | 5 | –314 | 4 | 2 | 0.552 | 0.019 | 0.998 | $8 \times 10^{-5}$ |
| | | | 0.046 | 164.8 | 0.2 | –180 | 7 | –296 | 4 | 1 | | | | |
| | | | 0.054 | –66.5 | 0.2 | –302 | 5 | –255 | 5 | 1 | | | | |
| | | Sta | 0.137 | 348.5 | 0.2 | –74 | 9 | –314 | 6 | 3 | 0.628 | 0.025 | 0.997 | $1 \times 10^{-5}$ |
| | | | 0.132 | 166.0 | 0.2 | –176 | 10 | –294 | 5 | 1 | | | | |
| | | | 0.134 | –64.5 | 0.2 | –329 | 10 | –283 | 7 | 2 | | | | |
| *T-$H_2$/$CO_2$ (calculated)* | | – | – | – | – | – | – | – | – | – | *0.707 ($f_W$=1)* | – | – | – |

[a] Thiosulfate-lactate (T-L); sulfate-lactate (S-L); thiosulfate-$H_2$/$CO_2$ (T-$H_2$/$CO_2$).
[b] Doubling time calculated for logarithmic growth.
[c] Biomass harvested during mid-exponential growth phase (Exp); biomass harvested during early stationary phase, including biomass from both exponential and stationary phase (Sta).
[d] Optical density (OD).
[e] $\delta^2H$ of culture medium at the time of biomass sampling. Average of biological and technical replicates ± 1 s.d.
[f] Weighted mean $\delta^2H$ of biphytane from GDGT-0.
[g] Number of biological replicates used to calculate the average values of $\delta^2H_{Water}$, $\delta^2H_{Lipid}$, and $^2\varepsilon_{L/W}$.
[h] Slope for the regression of $\delta^2H_{Lipid}$ against $\delta^2H_{Water}$ (*see* Fig. 1D-F).

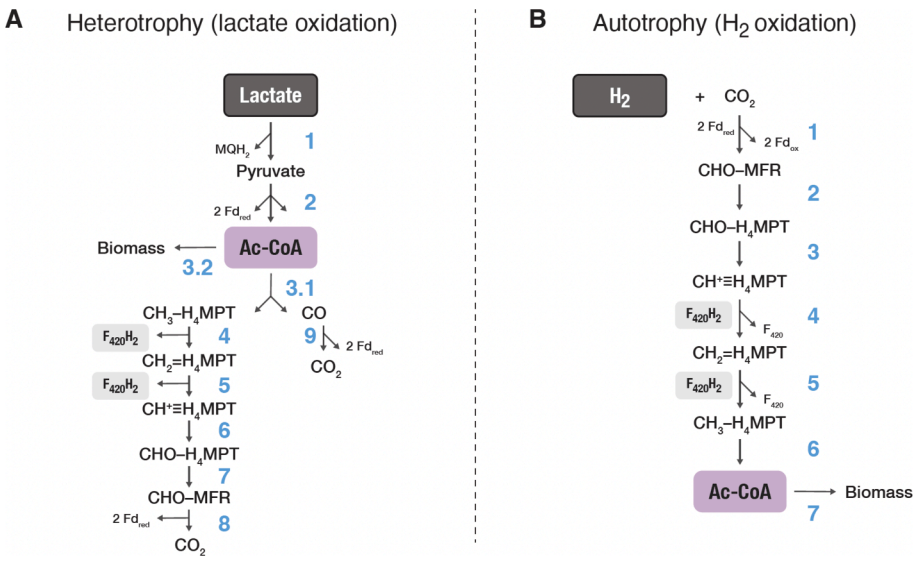


**Fig. 2.** Carbon metabolism by *Archaeoglobus fulgidus* via the modified reductive acetyl-CoA or Wood-Ljungdahl pathway. (A) Chemoorganoheterotrophic growth on lactate: lactate is oxidized via pyruvate and acetyl-CoA, which either serves as the building blocks for biosynthesis or is further degraded for the complete oxidation of lactate. (B) Chemolithoautotrophic growth on $H_2$/$CO_2$: $CO_2$ is reduced to produce acetyl-CoA via the $C_1$-pathway, with enzymes and cofactors similar to those involved in methanogenesis. Abbreviations: $MQH_2$, menaquinol or reduced menaquinone; $Fd_{red}$, reduced ferredoxin; Ac-CoA, acetyl-CoA; $CH_3$-$H_4$MPT, methyl-tetrahydromethanopterin ($H_4$MPT); $CH_2$ = $H_4$MPT, methylene-$H_4$MPT; $CH^+$≡$H_4$MPT, methenyl-$H_4$MPT; CHO-$H_4$MPT, formyl-$H_4$MPT; CHO-MFR, formylmethanofuran; $F_{420}H_2$, reduced coenzyme $F_{420}$.

considering the known mechanisms of how the enzymes of interest operate in methanogens. In $CO_2$-reducing methanogens, both methylenetetrahydromethanopterin reductase (Mer) and methylenetetrahydromethanopterin dehyrogenase (Mtd) oxidize $F_{420}H_2$ (Steps 4 and 5, respectively, in reverse; Fig. 2A), and formylmethanofuran dehydrogenase (Fwd) requires $Fd_{red}$ (Step 8, in reverse; Fig. 2A) (Thauer, 2012).

#### 4.1.2. Autotrophy

During chemolithoautotrophic growth *A. fulgidus* VC16 couples $H_2$ or formate oxidation with thiosulfate or sulfite reduction (Achenbach-Richter et al., 1987; Steinsbu et al., 2010). We fed *A. fulgidus* $H_2$ and thiosulfate as the electron donor and acceptor for the autotrophic condition (T-$H_2$/$CO_2$). *A. fulgidus* reduces $CO_2$ to synthesize Ac-CoA via the $C_1$-pathway (Fig. 2B), in principle a reversal of the Ac-CoA degradation

during heterotrophy (Fig. 2A). The same enzymes involved in H additions used by $CO_2$-reducing methanogens catalyze the successive addition of H during autotrophic carbon fixation in *A. fulgidus*: Fwd (Step 1), Mtd (Step 4), and Mer (Step 5) (Fig. 2B). During chemolithoautotrophy, the H atoms in methyl precursors in theory derive from intracellular water. However, the second reduction step catalyzed by Mtd (Step 4, Fig. 2B) can be alternatively catalyzed by an isoenzyme known as the $H_2$-forming methylene-$H_4$MPT dehydrogenase (Hmd) (Zirngibl et al., 1990; Von Bünau et al., 1991). While the $F_{420}$-reducing Mtd has a [NiFe] binuclear metal active site, the $H_2$-forming Hmd has a [Fe] mononuclear active site that allows the heterolytic cleavage of $H_2$ (Shima et al., 2008). Previous transcriptome analyses on hydrogenotrophic methanogens have revealed that Hmd is predominant during rapid growth under high partial pressures of $H_2$ (e.g., Pennings et al., 2000; Hendrickson et al., 2007). Given the similarities between methanogens and *A. fulgidus*, we consider the possible flux of H from $H_2$ to Ac-CoA (Step 4–6, Fig. 2B) in one of the end-member scenarios (see 4.2; Table 4).

### 4.2. Model schematics and stoichiometric accounting

Fractions of Ac-CoA produced via the modified Wood-Ljungdahl pathway described above are used for the synthesis of archaeal isoprenoids. Leavitt et al. (2023) provide a detailed overview of the sources of H and mechanisms of the biochemical steps involved in archaeal tetraether biosynthesis (Fig. S1). In short, the mevalonate pathway synthesizes isopentenyl pyrophosphate (IPP), which are $C_5$ isoprene units, from three units of Ac-CoA. Then, three units of IPP and its isomer condense to yield the $C_{20}$ precursor, geranylgeranyl diphosphate (GGPP). The geranylgeranyl chains are transferred around to yield di-O-geranylgenranylglyceryl phosphate (DGGGP) with the glycerol-1-phosphate (G1P) backbone. The tetraether synthase (Tes) enzyme catalyzes the condensation of two DGGGP units to yield the membrane-spanning tetraether. Finally, the geranylgeranyl reductase (GGR) enzyme catalyzes the saturation of tetraether to yield GDGT. We combine the stoichiometric accounting of the methyl-H in Ac-CoA for *A. fulgidus* (see 4.1) and of the 80 H atoms in the $C_{40}$ alkyl chain of BPs inherited from Ac-CoA during tetraether biosynthesis described above (Leavitt et al., 2023) to build an overall schematic of the specific model scenarios explored in this study (Fig. 3). All of the parameters used in the model schematic and the manuscript are summarized in Table 3.

#### 4.2.1. Empirically informed isotopic mass balance

With the fractions defined in the overall hydrogen budget (see Supplementary Material), the isotopic mass balance in Eq. (4) can be further refined. Replacing the $f_W$ and $f_S$ terms in Eq. (4) with the sums of all fractions in Eq. (S3) (Supplementary Material), isotopic mass balance for the heterotrophic condition becomes:

$$R_{BP,het} = \left(f_{W,direct}\cdot\alpha_{W,direct} + f_{W,indirect-LS}\cdot\alpha_{W,indirect-LS}\right)\cdot R_W + \left(f_{S,indirect-LS}\cdot\alpha_{S,indirect-LS} + f_{S-AS}\cdot\alpha_{S-AS}\right)\cdot R_S \quad (5)$$

Similarly, isotopic mass balance for the autotrophic condition becomes:

$$R_{BP,auto} = \left(f_{W,direct}\cdot\alpha_{W,direct} + f_{W,indirect-AS}\cdot\alpha_{W,indirect-AS} + f_{W,indirect-LS}\cdot\alpha_{W,indirect-LS}\right)\cdot R_W + f_{S-AS}\cdot\alpha_{S-AS}\cdot R_S \quad (6)$$

Now we can use the regression parameters estimated from the $\delta^2H_{H2O}$ label experiments (Fig. 1; Table 2) to calculate analytical solutions for reasonable ranges of individual terms in Eq. (5)–(6). In Eq. (5)–(6), the coefficient for $R_W$ in the first term represents the slope, $m$, and the entire second term represents the intercept, $c$. For heterotrophy:

$$m_{het} = f_{W,net}\cdot\alpha_{W,net} = f_{W,direct}\cdot\alpha_{W,direct} + f_{W,indirect-LS}\cdot\alpha_{W,indirect-LS}$$

$$\varepsilon_{W,net} = \left(\frac{m_{het}}{f_{W,net}} - 1\right)\bullet 1000$$

$$= \left(\frac{f_{W,direct}\cdot\alpha_{W,direct} + f_{W,indirect-LS}\cdot\alpha_{W,indirect-LS}}{f_{W,net}} - 1\right)\bullet 1000 \quad (7)$$

$$c_{het} = f_{S,net}\cdot\alpha_{S,net}\cdot R_S = f_{S,indirect-LS}\cdot\alpha_{S,indirect-LS} + f_{S-AS}\cdot\alpha_{S-AS}$$

$$\varepsilon_{S,net} = \left(\frac{c_{het}}{f_{S,net}\cdot R_S} - 1\right)\bullet 1000$$

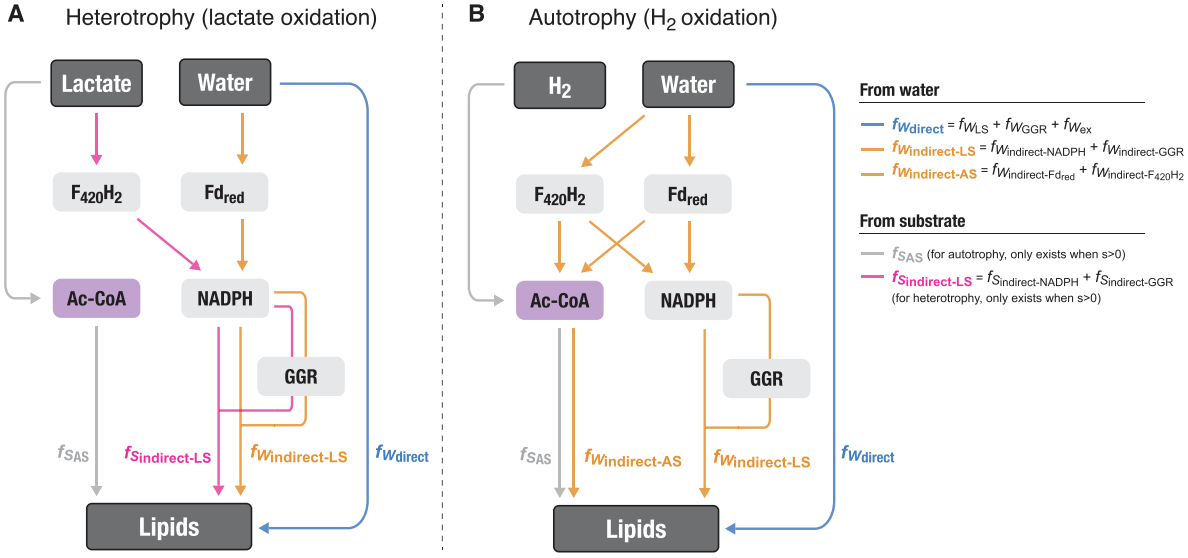


**Fig. 3.** Schematic diagram of the isotope flux-balance model for *Archaeoglobus fulgidus*. (A) Heterotrophic scenario for lactate oxidation; (B) autotrophic scenario for $H_2$ oxidation. Color codes for the different H fluxes ($f$) are shown in the legend. The subscript W stands for water as the ultimate H source; the subscript S stands for substrate as the ultimate H source, where the substrates are lactate and $H_2$ for heterotrophy and autotrophy, respectively. See 4.2.1 and Suppmentary Material (Eq. S3–S6) for detailed descriptions of individual fluxes. Abbreviations: LS, lipid synthesis; AS, acetyl-CoA synthesis; $F_{420}H_2$, reduced coenzyme $F_{420}$; $Fd_{red}$, reduced ferredoxin; Ac-CoA, acetyl-CoA; GGR, geranylgeranyl reductase.

**Table 3**
The definitions of parameters used in isotope flux balance model and throughout the manuscript. See 4.2 and Supplementary Material Fig. S1 for details.

| Parameter | Relevant metabolism(s) | H source | Definition & relevant processes |
|---|---|---|---|
| $f_W$ | both | water | Fluxes associated with any processes that are sourced from water |
| $f_{W,direct}$ | both | water | Fluxes sourced from water and associated with direct H exchange between water and lipid precursors |
| $f_{W,direct\text{-}LS}$ | both | water | Fluxes sourced from water and associated with general tetraether lipid biosynthesis (LS), with direct H exchange between water and lipid precursors |
| $f_{W,direct\text{-}GGR}$ | both | water | Fluxes sourced from water and associated with the gereanylgeranyl reductase (GGR) reduction step during tetraether lipid biosynthesis, with direct H exchange between water and lipid precursors |
| $f_{W,direct\text{-}Exch}$ | both | water | Fluxes sourced from water and associated with H isotope re-equilibration via isomerization during tetraether lipid biosynthesis, with direct H exchange between water and lipid precursors |
| $f_{W,indirect}$ | both | water | Fluxes sourced from water and associated with indirect H exchange between water and lipid precursors via cofactors during general tetraether lipid biosynthesis and/or acetyl-CoA biosynthesis |
| $f_{W,indirect\text{-}LS}$ | autotrophy | water | Fluxes sourced from water and associated with general tetraether lipid biosynthesis (LS), with indirect H exchange between water and lipid precursors via cofactors (e.g., $F_{420}$, ferredoxin, NADPH) |
| $f_{W,indirect\text{-}AS}$ | autotrophy | water | Fluxes sourced from water and associated with acetyl-CoA biosynthesis (AS), with indirect H exchange between water and lipid precursors via cofactors (e.g., $F_{420}$, ferredoxin, NADPH) |
| $f_S$ | both | substrate | Fluxes associated with any processes that are sourced from lactate (heterotrophy) or $H_2$ (autotrophy) |
| $f_{S,indirect\text{-}AS}$ | both | substrate | Fluxes sourced from lactate (heterotrophy) or $H_2$ (autotrophy) and associated with acetyl-CoA biosynthesis (AS), whose methyl-H's are incorporated into lipid precursors |
| $f_{S,indirect\text{-}LS}$ | heterotrophy | substrate | Fluxes sourced from lactate (heterotrophy) and associated with general tetraether lipid biosynthesis, where hydrides from lactate are transferred via coenzymes involved in the oxidative branch of acetyl-CoA degradation (e.g., $F_{420}H_2$ in Steps 4 and 5, Fig. 2A) during NADP reduction. The H in resulting NADPH ultimately traces back to lactate as the H source and can subsequently donate hydrides to lipid precursors |

$$= \left( \frac{f_{S,indirect-LS} \cdot \alpha_{S,indirect-LS} + f_{S-AS} \cdot \alpha_{S-AS}}{f_{S,net}} - 1 \right) \bullet 1000 \quad (8)$$

where $\varepsilon_{W,net}$ and $\varepsilon_{S,net}$ refer to the net isotope fractionation between water and lipid (combining isotope effects associated with $f_{W,direct}$ and $f_{W,indirect\text{-}LS}$) and between substrate and lipid (combining isotope effects associated with $f_{S,indirect\text{-}LS}$ and $f_{S\text{-}AS}$), respectively.

### 4.3. Model results

Table 4, Fig. 4 and Fig. 5 show the summary of model results. We first estimated $f_{W,net}$, which we define as the total flux that directly or indirectly (e.g., via cofactors) reflects water isotope composition (i.e., not affected by substrate isotopic composition) ($f_{W,net} = f_{W,direct} + f_{W,indirect}$), for a range of $x_{ex}$ from 0 % to 100 %. Overall, the autotrophic condition resulted in a higher range of $f_{W,net}$ compared to the two heterotrophic conditions (Table 4; Fig. 4A–C). Even for the minimal water exchange and maximal substrate contribution scenario ($x_{ex}$ = 0 %, $s$ = 100 %), when the contribution from substrate is expected to be the highest, $f_{W,net}$ was 80 % (Table 4; dashed line, Fig. 4A). For the two heterotrophic conditions, the $f_{W,net}$ values were 31 and 70 % for the highest ($x_{ex}$ = 0 %, $s$ = 100 %) and lowest ($x_{ex}$ = 100 %, $s$ = 0 %) substrate contribution scenarios, respectively (Table 4; Fig. 4B–C). Model results for the flux estimates of other parameters can be found in Figure S2.

For the net isotope fractionation between lipid and water ($\varepsilon_{W,net}$), the two heterotrophic conditions resulted in similar ranges and patterns where the $\varepsilon_{W,net}$ values decrease with increasing $x_{ex}$ (Fig. 4E–F). The $\varepsilon_{W,net}$ range was relatively more positive during stationary growth phase (–218 to 776 ‰ for the T-L condition; –259 to 682 ‰ for the S-L condition) compared to exponential growth phase (–312 to 561 ‰ for the T-L condition; –319 to 546 ‰ for the S-L condition) (Table 4; Fig. 4E–F). For the autotrophic condition, the growth phase-dependent trend was also observed (more positive $\varepsilon_{W,net}$ during stationary phase; Table 4; Fig. 4D). Unlike under heterotrophic conditions, all $\varepsilon_{W,net}$ values for the autotrophic condition were negative and fell within a relatively narrow range for the entire range of $x_{ex}$ (–448 to –312 ‰ for exponential phase; –372 to –228 ‰ for stationary phase; Table 4). For the autotrophic condition, a theoretical end-member $\varepsilon_{W,net}$ with no substrate contribution can be estimated by calculating the regression slope through the origin (i.e., no intercept, which represents the substrate contribution term, $f_S \cdot {}^2\alpha_{L/W} \cdot R_S$; Eq. (4)): –293 ‰ for the autotrophic condition (black dotted line; Fig. 4D). This value falls within the range of $\varepsilon_{W,net}$ for stationary, rather than exponential, growth phase (Fig. 4D). For the net isotope fractionation between lipid and substrate ($\varepsilon_{S,net}$), the two heterotrophic conditions resulted in similar ranges and patterns where $\varepsilon_{S,net}$ values increase with increasing $x_{ex}$ (Fig. 4H–I). The growth phase-dependent trend for $\varepsilon_{S,net}$ contrasted that of $\varepsilon_{W,net}$, where the $\varepsilon_{S,net}$ range was relatively more negative during stationary growth phase (–699 to –305 ‰ for the T-L condition; –665 to –227 ‰ for the S-L condition) compared to exponential growth phase (–595 to –67 ‰ for the T-L condition; –605 to –89 ‰ for the S-L condition) (Table 4; Fig. 4H–I). A similar trend was observed for the autotrophic condition (more negative $\varepsilon_{S,net}$ during stationary phase; Table 4; Fig. 4G).

The net isotope fractionation factors ($\varepsilon_{W,net}$ and $\varepsilon_{S,net}$) can be further broken down into individual fluxes associated with H isotopes with different routes of incorporation. The net isotope fractionation factor between lipid and water ($\varepsilon_{W,net}$) can be divided into: 1) $\varepsilon_{W,direct}$ associated with H atoms that are transferred through the $f_{W,direct}$ flux (Fig. 3) via H exchange between isoprenoid precursors and intracellular water or addition via GGR, and 2) $\varepsilon_{W,indirect}$ associated with the $f_{W,indirect}$ flux ($f_{W,indirect\text{-}LS}$ for heterotrophy; $f_{W,indirect\text{-}LS}$ and $f_{W,indirect\text{-}AS}$ for autotrophy; Fig. 3) via cofactors ($Fd_{red}$ and $F_{420}H_2$ for autotrophy; $Fd_{red}$ for heterotrophy) (Fig. 5A–C). The net isotope fractionation factor between lipid and substrate ($\varepsilon_{S,net}$) can be divided into: 1) $\varepsilon_{S\text{-}AS}$ associated with H atoms that are transferred through the $f_{S\text{-}AS}$ flux (Fig. 3) via Ac-CoA synthesis, and 2) $\varepsilon_{S,indirect}$ associated with the $f_S$ fluxes ($f_{S,indirect\text{-}NADPH}$ and $f_{S,indirect\text{-}GGR}$ for heterotrophy; Fig. 3) via cofactors ($F_{420}H_2$) (Fig. 5D–E). Interpretation of these results are discussed further in 5.2.1.

**Table 4**
Isotope flux-balance model results for *Archaeoglobus fulgidus*.

| Growth phase | Scenario | | $f_{W,net}$ (%)[c] | | | $\varepsilon_{W,net}$ (‰)[d] | | | $\varepsilon_{S,net}$ (‰)[e] | | |
|---|---|---|---|---|---|---|---|---|---|---|---|
| | $x_{ex}$ (%)[a] | $s$ (%)[b] | T-L | S-L | T-H | T-L | S-L | T-H | T-L | S-L | T-H |
| Exp. | 0 | 0 | 41 | 41 | 100 | 179 | 167 | –448 | –527 | –538 | n/a |
| | 0 | 100 | 31 | 31 | 80 | 561 | 546 | –312 | –595 | –605 | –564 |
| | 100 | 0 | 70 | 70 | 100 | –312 | –319 | –448 | –67 | –89 | n/a |
| | 100 | 100 | 60 | 60 | 90 | –198 | –206 | –387 | –300 | –317 | –139 |
| Sta. | 0 | 0 | 41 | 41 | 100 | 341 | 270 | –372 | –648 | –608 | n/a |
| | 0 | 100 | 31 | 31 | 80 | 776 | 682 | –218 | –699 | –665 | –785 |
| | 100 | 0 | 70 | 70 | 100 | –218 | –259 | –372 | –305 | –227 | n/a |
| | 100 | 100 | 60 | 60 | 90 | –87 | –136 | –302 | –479 | –420 | –577 |

[a] the degree of water exchange during lipid synthesis, which depends on the extent of re-equilibration during isomerization steps (Steps 2 and 6; Fig. S1).
[b] the degree of H contribution to lipids from substrate (lactate for heterotrophy; $H_2$ for autotrophy).
[c] the net total contribution of H from water to lipids ($f_{W,net} = f_{W,direct} + f_{W,indirect}$).
[d] the net isotope fractionation between water and lipid (combining isotope effects associated with $f_{W,direct}$ and $f_{W,indirect\text{-}LS}$).
[e] the net isotope fractionation between substrate and lipid (combining isotope effects associated with $f_{S,indirect\text{-}LS}$ and $f_{S,AS}$).

## 5. Discussion

### 5.1. Isotopic re-equilibration via isomerization during archaeal isoprenoid lipid biosynthesis

The model results show all possible solutions within the set bounds of modeled parameters (Figs. 4 and 5; Table 4). To further constrain ranges of more plausible solutions under our experimental conditions, we can make additional biologically informed assumptions. For example, the extent of solution space in our model is determined by the degree of water isotope exchange ($x_{ex}$) during isomerization (Steps 2 and 6, Fig. S1), which ranges from 0 to 100 %. The four end-member scenarios are set as either minimal exchange scenario ($x_{ex}$ = 0 %; no isotopic re-equilibration) or maximal exchange scenario ($x_{ex}$ = 100 %; 24 out of 80 H's in biphytane isotopically equilibrate with water) to explore the full range of possible solutions (Table 4). What would be the range of $x_{ex}$ values that is more plausible considering the experimental conditions and our knowledge about the physiology of *A. fulgidus*?

While $x_{ex}$ is allowed to range from 0 to 100 %, it is unlikely that $x_{ex}$ is very low or 0 % given that genes encoding enzymes that catalyze the isomerization steps (acetyl-CoA acetyl transferase or thiolase, Step 2; isopentenyl pyrophosphate isomerase, Step 6; Fig. S1) are constitutively highly expressed in *A. fulgidus* (Hocking et al., 2014). For example, the gene expression level for acetyl-CoA acetyl transferase which can catalyze the tautomerization of acetoacetyl-CoA (Step 2; Fig. S1) was *ca.* 3-fold higher compared to the mean for all assayed genes under similar growth conditions as those tested in this study (T-L, S-L and T-$H_2$/$CO_2$; exponential and late-exponential conditions; (Hocking et al., 2014). Thus, $x_{ex}$ is most likely a non-zero value for *A. fulgidus* cultures under our experimental conditions and non-negligible isotopic re-equilibration between water and lipid precursors can be rationalized.

Constraints on the range of $x_{ex}$ ultimately define the direction and magnitude of net isotope fractionation between lipid and water ($\varepsilon_{W,net}$), as $\varepsilon_{W,net}$ is determined by the relative ratio between the slope of the regression line ($m$) and the total flux that reflects water isotope composition ($f_{W,net}$):

$$\alpha_{W,net} = \frac{m}{f_{W,net}} \quad (9)$$

Normal kinetic isotope fractionation ($\varepsilon_{W,net} < 0$; $\alpha_{W,net} < 1$) would be expected when $m$ is a smaller positive number compared to $f_{W,net}$. At $x_{ex}$ = 50 %, $f_{W,net}$ values range from 0.45 (s = 100 %) to 0.55 (s = 0 %) for heterotrophy (Fig. 4B and 4C); from 0.85 (s = 100 %) to 1 (s = 0 %) for autotrophy (Fig. 4A). The range of slope terms measured for the autotrophic condition ($m$ = 0.552–0.628; Table 2) entirely falls below the $f_{W,net}$ range for autotrophy, suggesting negative $\varepsilon_{W,net}$ values in all cases. Some, not all, of the slope terms measured for the heterotrophic condition ($m$ = 0.481–0.548 for T-L; $m$ = 0.477–0.519 for T-L; Table 2) are lower than the $f_{W,net}$ range for heterotrophy; at $x_{ex}$ = 100 %, the range of slope terms for heterotrophy entirely falls below the $f_{W,net}$ range for heterotrophy (0.60 at s = 100 %; 0.70 at s = 0 %; Fig. 4B and 4C; Table 3), which would result in negative $\varepsilon_{W,net}$ values. Altogether, normal kinetic isotope fractionation (negative $\varepsilon_{W,net}$) is plausible under all autotrophic conditions and most heterotrophic conditions for *A. fulgidus*, assuming isotopic re-equilibration via isomerization during lipid synthesis. We carry the assumption of negative $\varepsilon_{W,net}$ throughout the remainder of Discussion below for further interpretation.

### 5.2. Effects of carbon metabolism and growth phase on lipid H isotope composition in Archaea

The isotope flux-balance model results show a large fraction of lipid-H directly reflects water H isotope compositions, rather than substrate (lactate or $H_2$) isotope compositions in *A. fulgidus*. We observe higher $f_{W,net}$ for autotrophic growth ($f_{W,net}$ = 80–100 %), whereas $f_{W,net}$ for heterotrophic growth was lower ($f_{W,net}$ = 31–70 %; Table 4; Fig. 4A–C). Assuming normal kinetic isotope fractionation (*see* 5.1), we can constrain the $f_{W,net}$ range that corresponds to $\varepsilon_{W,net} < 0$ (*see* Fig. 4D–E). This yields $f_{W,net}$ ranges of: 38–52 % for T-L and 42–52 % for S-L during exponential growth phase, versus 50–56 % for T-L and 52–54 % S-L during stationary growth phase. The lowest $f_{W,net}$ recorded were during heterotrophy in exponential phase, independent of the terminal electron acceptor. For stationary phase cultures of *A. fulgidus*, the $f_{W,net}$ was ≥ 80 % for autotrophy versus ≥ 50 % for heterotrophy. The $f_{W,net}$ range for lipids produced during stationary phase alone is likely larger, because lipids collected during stationary phase are a mixture of those produced during exponential phase and those newly produced during stationary phase. The higher $f_{W,net}$ range observed for autotrophy is reasonable, given that lactate is an additional source of H that contributes directly to Ac-CoA synthesis during heterotrophy. Interestingly, a similar observation was reported for bacterial fatty acids where, for instance, the mole fraction of lipid H derived from water (≡ $X_W$ in Zhang et al., 2009; herein equivalent to $f_{W,net}$) was larger for *Escherichia coli* grown on glucose compared to the same organism grown on complex medium (Zhang et al., 2009). Though the lipid synthesis pathways are different for Bacteria versus Archaea, it appears that the fractional contribution of substrates that are more direct precursors for lipid biosynthesis generally increases when organic substrates are used or $H_2$ is supplied in excess as an electron donor.

The effects of carbon metabolism and growth phase on lipid isotope composition have not been investigated in detail for archaeal lipids. Our results indicate that both the mode of metabolism and growth phase affect the lipid isotope composition (Table 4; Fig. 4). A recent study reported $\varepsilon_{L/W}$ of BPs produced by *N. maritimus* in continuous cultures at

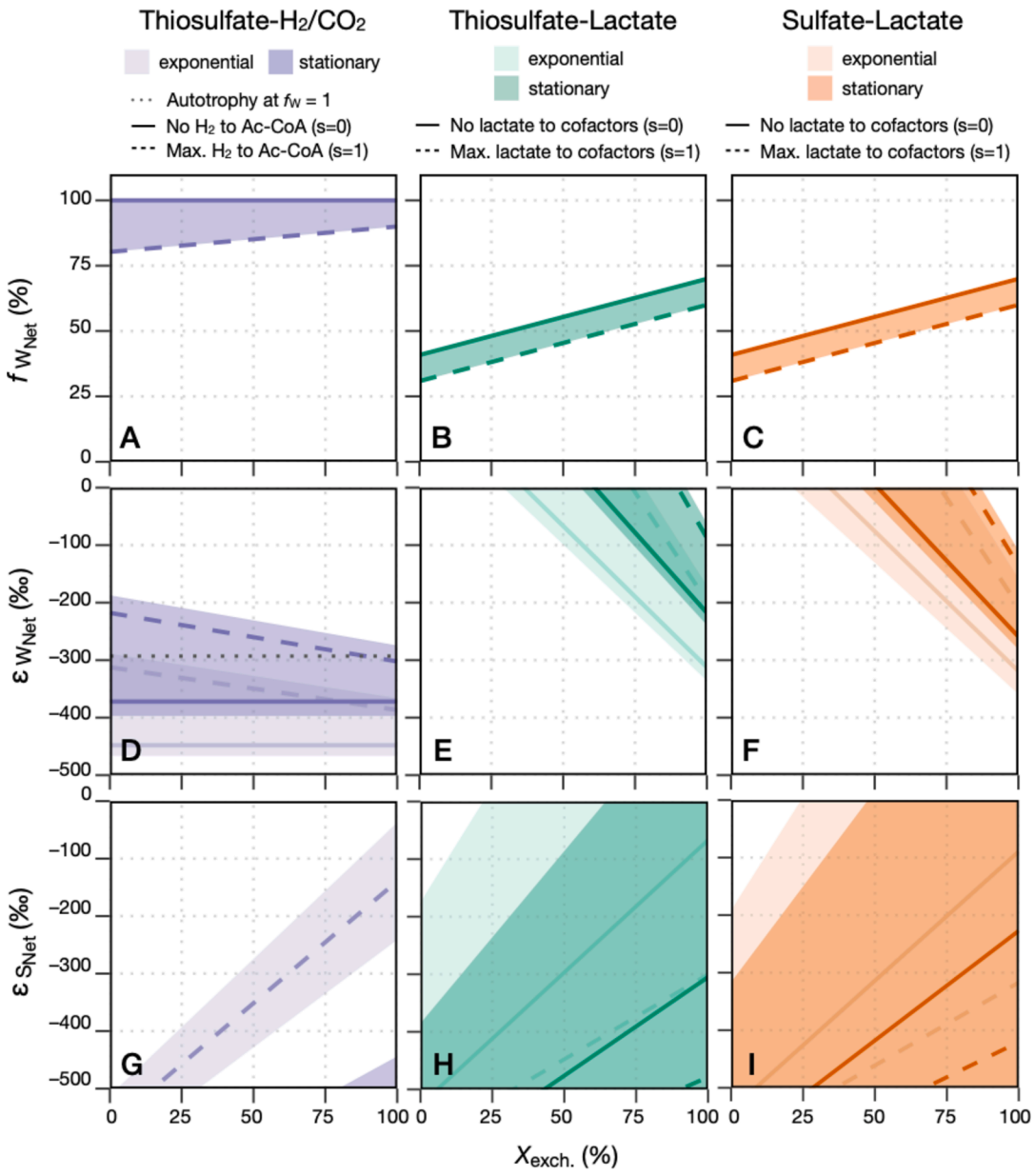


**Fig. 4.** Isotope flux-balance model results for *Archaeoglobus fulgidus*. (A–C) The total flux that directly or indirectly (e.g., via cofactors) reflects water isotope composition (i.e., not affected by substrate isotopic composition) ($f_{W,net}$); (D–F) Net isotope fractionation between lipid and water ($\varepsilon_{W,net}$); (G–I) Net isotope fractionation between lipid and substrate ($\varepsilon_{S,net}$). Each column represents the metabolic mode and growth substrates: autotrophy on thiosulfate and $H_2/CO_2$ (A, D and G); heterotrophy on thiosulfate and lactate (B, E and H); and heterotrophy on sulfate and lactate (C, F and I). Lighter shaded areas refer to exponential growth phase; darker shades refer to stationary growth phase. Solid lines refer to the s = 0 % (minimal substrate contribution) scenarios; dashed lines refer to the s = 100 % (maximal substrate contribution) scenarios. See 4.2.1 and Table 4 for details of the conditions for each scenario.

a range of doubling time and observed little change in $\varepsilon_{W/L}$ (0.18 ± 0.09 ‰ increase in $\varepsilon_{L/W}$ per hour increase in doubling time; Leavitt et al., 2023). The relative variation in doubling time we observe for *A. fulgidus* grown on different substrates here in batch cultures (Table 2) is similar (*ca.* 3-fold variation) to the variation observed for *N. maritimus* in Leavitt et al. (2023). A key difference here is that we do not strictly control growth and metabolic rates, as was the case for chemostat cultivation of *N. maritimus* (Leavitt et al., 2023). Nonetheless, the range of $\varepsilon_{L/W}$ we observe across different metabolic modes by *A. fulgidus* (–231 ± 6 ‰ for T-L, –241 ± 4 ‰ for S-L, and –271 ± 18 ‰ for T-$H_2/CO_2$; Table 2) is large compared to the entire range of $\varepsilon_{L/W}$ observed across a similar variation in growth rate by *N. maritimus* (–272 ± 20 to –279 ± 8 ‰ for BP-0; Leavitt et al., 2023). *N. maritimus* is an obligate chemoautotroph, such that all BP-bound H is strictly biosynthetic, whereas we show here that patterns of $\varepsilon_{W/L}$ can change between heterotrophic and autotrophic growth conditions (Fig. 4 and Fig. 6). Our results support this hypothesis and show variation in $\varepsilon_{L/W}$ up to ~ 40 ‰ within the same metabolically versatile organism, in response to different electron donor–acceptor pairs and modes of carbon metabolism.

### 5.3. *Factors that affect lipid-water H isotope fractionation across the three domains of life*

Here we present a synthesis of the broader $\varepsilon_{L/W}$ patterns observed in lipids from all three domains of life. Archaeal isoprenoid lipids are characterized by a relatively narrow range of large and negative values of $\varepsilon_{L/W}$ across a wide range of organisms, metabolisms, and growth conditions (Fig. 6; Kaneko et al., 2011; Wu et al., 2020; Leavitt et al.,

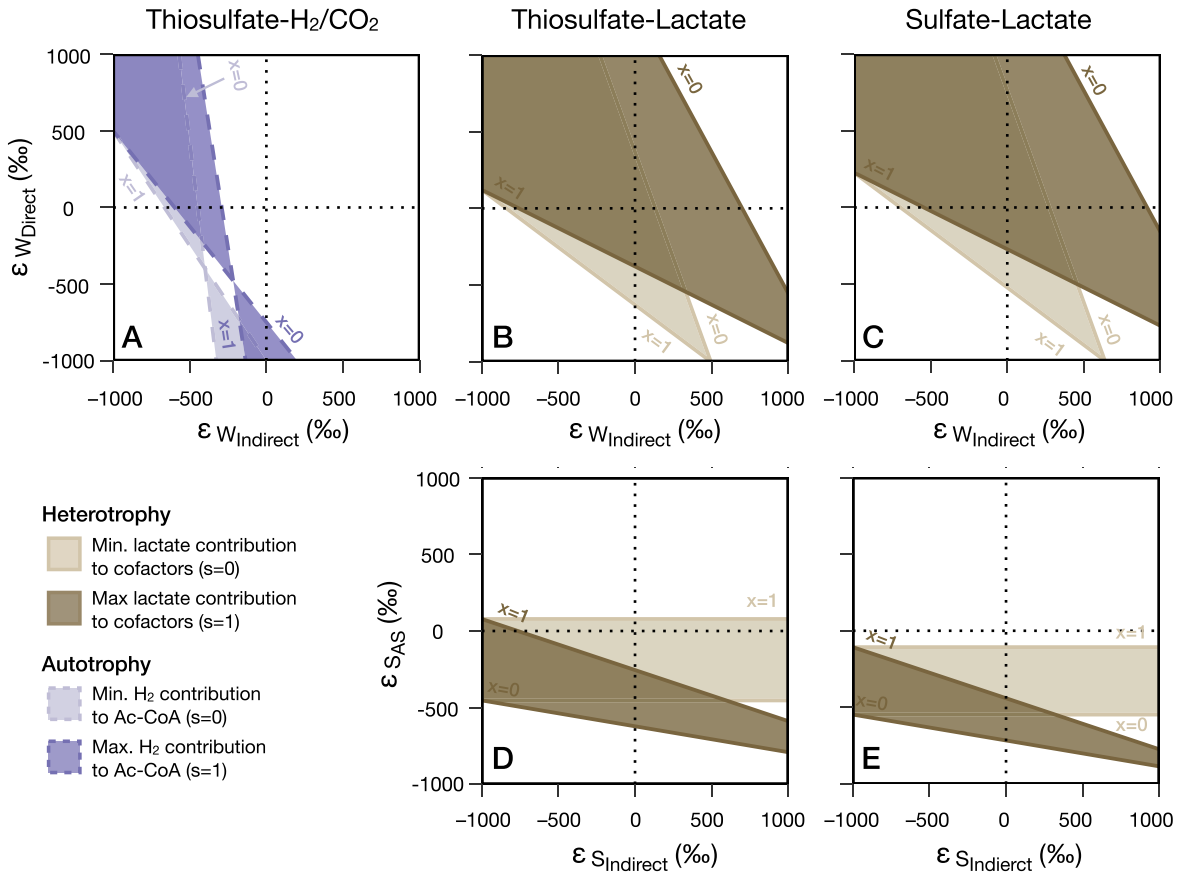


**Fig. 5.** Isotope flux-balance model results for *Archaeoglobus fulgidus*. (A–C) Breakdown of the net isotope fractionation between lipid and water ($\varepsilon_{W,net}$; Fig. 4D–F) into two different isotope fractionation factors: $\varepsilon_{W,direct}$ for H atoms that are transferred through exchange during isomerization or addition via GGR, corresponding to $f_{W,direct}$ in Fig. 3, and $\varepsilon_{W,indirect}$ for H atoms that are transferred through cofactors ($Fd_{red}$ and $F_{420}H_2$ for autotrophy, panel A; $Fd_{red}$ for heterotrophy, panels B and C), corresponding to $f_{W,indirect}$ in Fig. 3. (D–E) Breakdown of the net isotope fractionation between lipid and substrate ($\varepsilon_{S,net}$; Fig. 4G–I) into two different isotope fractionation factors: $\varepsilon_{S,AS}$ for H atoms that are inherited directly from substrate via Ac-CoA, corresponding to $f_{S,AS}$ in Fig. 3, and $\varepsilon_{S,indirect}$ for H atoms that are transferred through cofactors (only applicable for heterotrophy via $F_{420}H_2$, panels D and E), corresponding to $f_{S,indirect}$ in Fig. 3. The lighter shaded areas refer to the s = 0 % (minimal substrate contribution) scenarios; darker shaded areas refer to the s = 100 % (maximal substrate contribution) scenarios. Solid lines and brown colors refer to heterotrophic conditions; dashed lines and purple colors refer to autotrophic conditions. See 4.2.1 and Table 4 for details of the conditions for each scenario.

2023; this study). This is in contrast with observations in bacterial fatty acids (main constituents of membrane lipids in the domain Bacteria), where measured $\varepsilon_{L/W}$ values range a large span of > 600 ‰ with both highly positive and negative values (Fig. 6; Campbell et al., 2009; Zhang et al., 2009; Dawson et al., 2015; Osburn et al., 2016; Wijker et al., 2019). Archaeal isoprenoid lipid $\varepsilon_{L/W}$ largely overlaps with that of eukaryotic isoprenoid lipid $\varepsilon_{L/W}$, although the latter spans a significant range depending on the types of eukaryotes, classes of compound and corresponding biosynthetic pathways (Fig. 6; Sessions et al., 1999; Chikaraishi et al., 2004, 2009; Zhang and Sachs, 2007; Sachs et al., 2016). Notably, there are subgroups of both domains Bacteria and Eukarya that share similarities with Archaea in their $\varepsilon_{L/W}$. The shared similarities are interesting, given the difference in lipid biosynthesis mechanism among the three domains. Below, we take a closer look at the specific subsets of $\varepsilon_{L/W}$ values from the domains Euakarya and Bacteria that resemble those from Archaea and discuss factors that may contribute to the large, negative values of $\varepsilon_{L/W}$ observed across the three domains.

### 5.3.1. *Potential mechanisms underlying large H isotope fractionation in archaeal and eukaryotic isoprenoid lipids*

The consistently large, negative values of $\varepsilon_{L/W}$ for archaeal lipids are notable considering the different types of organism and metabolic modes studied so far (Fig. 6). In Fig. 5, we present the model solution spaces for individual H fluxes, within either net flux that reflects water isotope composition (i.e., not affected by substrate contributions; $f_{W,net}$) or net flux that reflects isotopic contributions from organic substrate or $H_2$ ($f_{S,net}$), to further investigate specific parts of archaeal lipid biosynthesis pathway that may contribute to the observed large and negative values of $\varepsilon_{L/W}$. Prior work yielded estimates of $\alpha_W \cong 0.9$ for isotope fractionation associated with direct water incorporation across many bacteria (Zhang et al., 2009; Wijker et al., 2019). It is important to note that the $\alpha_W$ value of 0.9 was estimated from a model for bacterial fatty acids, and the $\alpha_W$ value for archaeal isoprenoids may be different. The only existing hydrogen isotope model for archaeal isoprenoids, however, yielded modeled parameters that are most consistent with experimental observations with *N. maritimus* cultures when the value of $\alpha_W$ was set to 0.9; assuming $\alpha_{NADPH}<1$, smaller $\alpha_W$ values (larger fractionation) resulted in unreasonably high estimates of $\alpha_{ETC}$ (Leavitt et al., 2023). Applying an equivalent assumption for our model would be setting the value of $\varepsilon_{W,direct}$ at –100 ‰. Under this assumption the range of $\varepsilon_{W,indirect}$ is particularly well constrained for the autotrophic condition (–599 to –436 ‰ at $s$ = 0 %; –519 to –276 ‰ at $s$ = 100 % when $\varepsilon_{W,direct}$ = –100 ‰; Fig. 5A). Even if $\alpha_W$ was smaller (more negative value of $\varepsilon_{W,direct}$) for archaeal isoprenoids, the modeled values of $\varepsilon_{W,indirect}$ would suggest significant negative isotope fractionation (e.g., $\varepsilon_{W,indirect}$ = –332 to –387 ‰ at $s$ = 0 %; –200 to –213 ‰ at $s$ = 100 % when $\varepsilon_{W,direct}$ = –100 ‰; Fig. 5A).

It is plausible that both $\varepsilon_{W,indirect\text{-}AS}$ and $\varepsilon_{W,indirect\text{-}LS}$ have negative values that are comparable to the combined value of $\varepsilon_{W,indirect}$, as the less

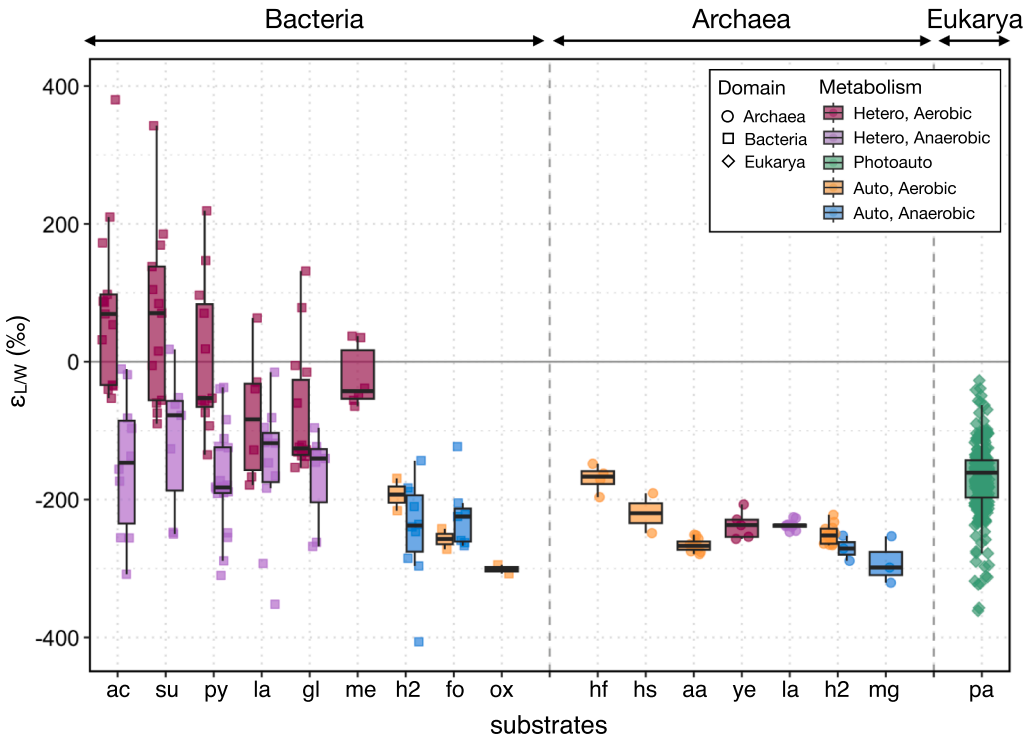


**Fig. 6.** Summary of hydrogen isotope fractionation ($\varepsilon_{L/W}$) between lipids and water observed in culture studies. $\varepsilon_{L/W}$ values observed in all three domains of life: Archaea (circle), Bacteria (square), and Eukarya (diamond). Color codes represent different types of metabolism: aerobic heterotrophy (red), anaerobic heterotrophy (purple), oxygenic photoautotrophy (green), aerobic chemoautotrophy (orange), and anaerobic chemoautotrophy (blue). Electron donors used for biosynthesis are shown on the horizontal axis: acetate (ac); succinate (su); pyruvate (py); lactate (la); glucose (gl); methane (me); $H_2 + CO_2$ (h2); formate (fo); oxalate (ox); $H_2 + Fe^{3+}$ (hf); $H_2 + S^0$ (hs); ammonium (aa); yeast extract (ye); $H_2$, acetate or methanol for methanogenesis (mg); water for photoautotrophy (pa). Tested organisms for bacterial cultures include *C. oxalaticus*, *C. necator*, *R. palustris* (Zhang et al., 2009); *E. coli* (Zhang et al., 2009; Osburn et al., 2016; Wijker et al., 2019); *D. autotrophicum* (Campbell et al., 2009; Osburn et al., 2016); *M. capsulatus* (Sessions et al., 2002); *D. multivorans* (Dawson et al., 2015); *D. alaskensis* (Leavitt et al., 2016); *P. denitrificans*, *S. oneidensis*, *D. hydrogenophilus*, *D. alaskensis*, *D. propionicus* (Osburn et al., 2016); *Sporomusa* sp. (Valentine et al., 2004); *B. subtilis*, *P. fluorescens*, *R. radiobacter*, and *E. meliloti* (Wijker et al., 2019). Tested organisms for eukaryotic cultures include *A. fundyense*, *I. galbana*, *Ascophyllum* sp., *F. vesiculosis*, *Z. marina*, *S. alterniflora* (Sessions et al., 1999); *C. japonica* (Chikaraishi et al., 2004); *B. braunii*, *E. unicocca*, *V. aureus* (Zhang and Sachs, 2007); *C. sativuc* (Chikaraishi et al., 2009); *E. huxleyi* (Sachs et al., 2016). Tested organisms for archaeal cultures include *Acidianus* sp. DS80 (this study); *N. maritimus* (Leavitt et al., 2023); *Sulfolobus* sp. (Kaneko et al., 2011); *A. fulgidus* (this study); *Metallosphaera sedula* (this study); and *M. barkeri* (Wu et al., 2020).

likely alternative would be a negative $\varepsilon_{W,indirect}$ that consists of very different $\varepsilon_{W,indirect\text{-}AS}$ and $\varepsilon_{W,indirect\text{-}LS}$. Our current model cannot distinguish between isotope fractionation factors associated with different fluxes within $f_{W,indirect}$ (i.e., $f_{W,indirect\text{-}AS}$ through Ac-CoA *vs.* $f_{W,indirect\text{-}LS}$ through NADPH), both of which can inherit H from cofactors $F_{420}H_2$ and/or $Fd_{red}$ (Fig. 3B). However it is worth noting that, for both heterotrophic and autotrophic conditions, a fraction of the $f_{W,indirect\text{-}LS}$ flux represents hydride transfer during the final saturation (double bond reduction) via GGR (Fig. 3; Step 10, Fig. S1). Below, we examine the details of both direct ($f_{W,direct}$) and indirect ($f_{W,indirect}$) routes of hydrogen incorporation to further elucidate potential mechanisms of $^2H$ depletion in *A. fulgidus* observed in this study as well as other archaea and eukaryotes with similar $\varepsilon_{L/W}$ patterns.

A closer examination of the eukaryotic lipids that share similar $\varepsilon_{L/W}$ values with archaeal lipids suggests two likely sources of $^2H$ depletion: 1) isomerization steps shared commonly among general isoprenoid biosynthesis pathways and 2) the GGR reduction step that imposes additional $^2H$ depletion in saturated acyclic isoprenoids. Fig. 7A shows $\varepsilon_{L/W}$ for different subgroups of eukaryotic lipids, categorized by three different biosynthetic pathways: acetogenic, MVA and MEP pathways. All Archaea discussed in this study synthesize isoprenoid lipids via the MVA pathway. The MEP pathway is generally defined as bacterial and the MVA pathway as eukaryotic and archaeal; both pathways often simultaneously occur in plants, where the MEP pathway is expressed in chloroplasts (relics of the cyonobacterial plastid ancestor) and the MVA pathway is expressed in the cytosol (Lichtenthaler et al., 1997; Lichtenthaler, 1999; Pearson, 2014). An exception to this is the case of green algae, where both the cytosolic sterols and plastidic phytol isoprenoids are synthesized via the MEP pathway (Lichtenthaler et al., 1997; Disch et al., 1998; Pearson, 2014).

The three different biosynthetic pathways of eukaryotic lipids (acetogenic, MVA, and MEP) are associated with distinct ranges of $\varepsilon_{L/W}$ where isoprenoid lipids are generally more depleted in $^2H$ compared to acetogenic lipids (*see* Introduction). This general trend is captured in Fig. 7A, where acetogenic lipids (e.g., *n*-alkanol and *n*-alkyl lipids including fatty acids) have more positive $\varepsilon_{L/W}$ compared to isoprenoid lipids. The $C_{15}$ and $C_{30}$ isoprenoids synthesized via the MVA pathway (e.g., sterol, triterpenoids, sesquiterpenes, squalene) are relatively more enriched in $^2H$ compared to the $C_{20}$ isoprenoids (e.g., phytol, phytadiene, diterpenes) and botryococcenes (triterpenes) synthesized via the MEP pathway (Fig. 7A). The range of $\varepsilon_{L/W}$ values for archaeal diethers and tetraethers largely overlaps with the range for eukaryotic $C_{15}$ and $C_{30}$ isoprenoids and partially overlaps with generally more negative $\varepsilon_{L/W}$ values for the eukaryotic isoprenoids synthesized via the MEP pathway (Fig. 7A). Organisms that produce these isoprenoid lipids vary widely in their carbon and energy metabolism, from eukaryotic photoautotrophs to archaea as well as various types of metabolism among archaea (aerobic/anaerobic heterotrophy and aerobic/anaerobic autotrophy; Fig. 7A). Thus, the mechanisms underlying $^2H$ depletion in eukaryotic and archaeal isoprenoid lipids most likely reflect core biochemical steps involved in isoprenoid biosynthesis.

Considering that the compared isoprenoids with similar $\varepsilon_{L/W}$ values

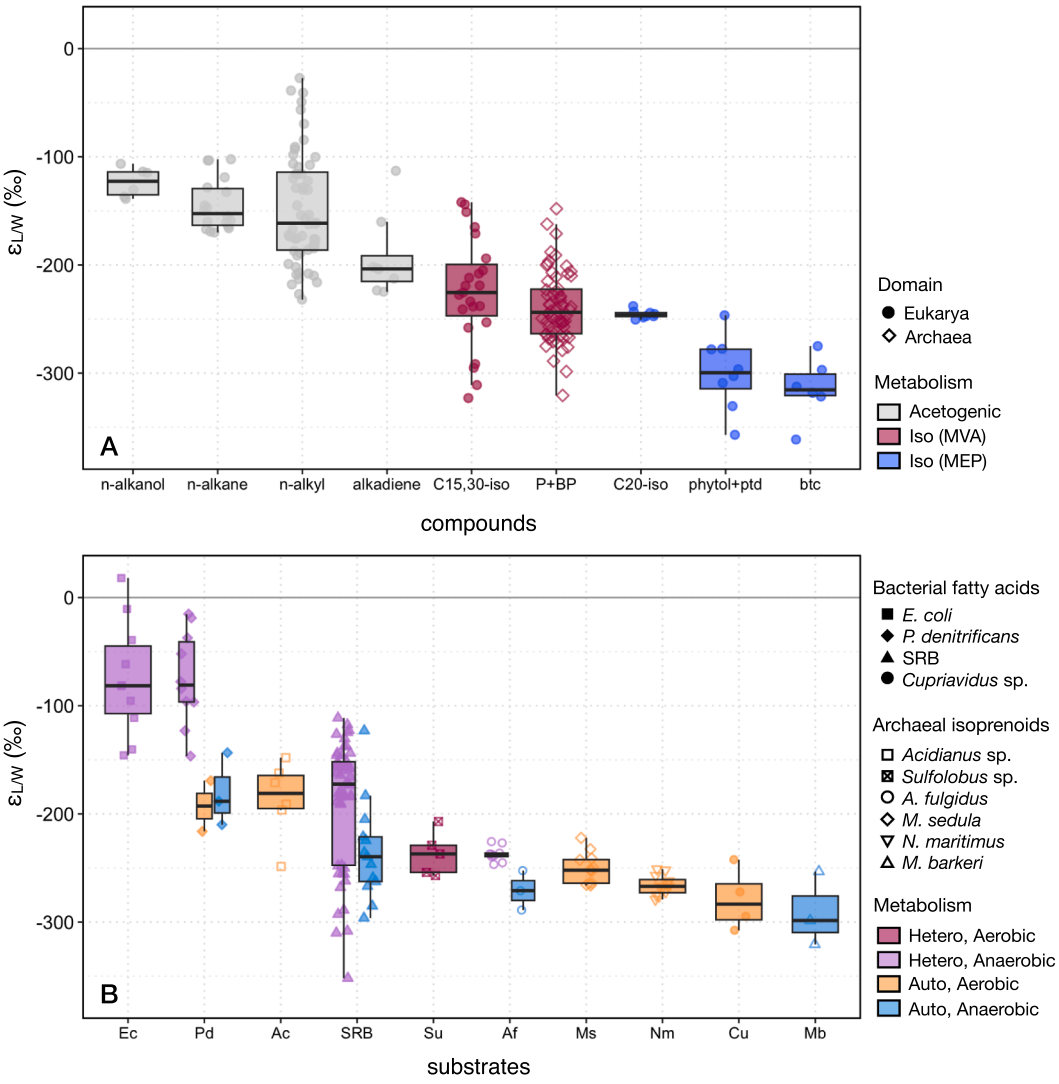


**Fig. 7.** Comparison of $\varepsilon_{L/W}$ values observed in eukaryotic *vs*. archaeal lipids and in bacterial *vs*. archaeal lipids. **(A)** $\varepsilon_{L/W}$ values observed in acetogenic and isoprenoid lipids from the domains Archaea and Eukarya. Different classes of compounds are shown on the horizontal axis. Compounds shown for acetogenic pathway: n-alkanol, *n*-alkane, *n*-alkyl (*n*-alkanoic acids and fatty acids), and alkadiene. For the MVA pathway: $C_{15}$ and $C_{30}$ isoprenoids (sterol, squalene, triterpenoids, and sesquiterpenes) and P+BP (phytanes and biphytanes). For the MEP pathway: $C_{20}$ isoprenoids (diterpenes, sandaracopimarinol, ferruginol, diterpenol, and sugiol), phytol + ptd (phytol and phytadiene), and btc (botryococcene). **(B)** $\varepsilon_{L/W}$ values observed in fatty acids from anaerobic and/or autotrophic Bacteria and isoprenoid lipids from Archaea. Different organisms are shown on the horizontal axis. For Bacteria: *E. coli* (Ec), *Paracoccus denitrificans* (Pd), SRB (*Desulfobacterium autotrophicum*, *Desulfococcus multivorans*, *Desulfobacter hydrogenophilus*, *Desulfovibrio alaskensis*, *Desulfolobus propionicus*), and *Cupriavidus* sp. (Cu). For Archaea: *Acidianus* sp. DS80 (Ac), *Sulfolobus* sp. (Su), *Archaeoglobus fulgidus* (Af), *Metallosphaera sedula* (Ms), *Nitrosopumilus maritimus* (Nm), and *Methanosarcina barkeri* (Mb). A full list of references can be found in Supplementary Material.

include diverse compounds with different carbon chain lengths (from $C_{15}$ to $C_{40}$) and structures (from linear terpenes to cyclic products), we propose that the generally large negative $\varepsilon_{L/W}$ values observed across a range of eukaryotic and archaeal isoprenoids likely reflect isotope exchange via isomerization step(s) during the early part of isoprenoid biosynthesis involving five-carbon building blocks and intermediates. Such processes would be the two isomerization steps: 1) tautomerization of acetoacetyl-CoA with isotope exchange at the $C_2$ position and 2) isomerization of isopentenyl pyrophosphate with isotope exchange at the $C_4$ position (Steps 2 and 6; Fig. S1). As discussed in 5.1, these isomerization steps can result in significant isotope re-equilibration (up to 24 out of 80 H's per biphytane molecule at $x_{ex}$ = 100 %; Table 4; Fig. S1).

Among the $^2$H-depleted isoprenoid lipids, compounds with particularly more negative $\varepsilon_{L/W}$ values likely have additional biochemical mechanisms with large isotope effects involved in downstream biosynthetic pathways. In fact, the larger and more negative values of $\varepsilon_{L/W}$ appear to correlate more with highly fractionating enzymatic steps, rather than specific pathways (i.e., MVA *vs*. MEP). For example, Chikaraishi et al. (2004) observed in *Cryptomeria japonica* (conifer) that $\varepsilon_{L/W}$ values for cytosolic lipids produced via the MVA pathway, sesquiterpenes (–228 to –238 ‰) and squalene (–225 to –251 ‰), are similar to those for plastidic diterpenoids (–238 to –251 ‰) produced via the MEP pathway (Fig. 7A). Phytol and botryococcenes, on the other hand, have particularly negative $\varepsilon_{L/W}$ values among eukaryotic lipids produced via the MEP pathway. For example, Zhang and Sachs (2007) found that botryococcenes with longer chain lengths had progressively lower $\delta^2$H compared to the $C_{30}$ botryococcene (precursor to all other botryococcenes) in *Botryococcus braunii* race B. They hypothesized that significantly $^2$H-depleted hydrogen from methionine is incorporated into botryococcene during the step-wise methylation (Zhang and Sachs, 2007). Similarly, phytol in *C. japonica* had up to 65 ‰ more negative $\varepsilon_{L/W}$ compared to diterpenoids, another plastidic lipid produced via the MEP pathway within the same organism (Chikaraishi et al., 2004). Later,

Chikaraishi et al. (2009) observed a gradual depletion in $\delta^2H$ from phytol precursors (starting from geranylgeraniol) to phytol in cucumber, indicating that significantly $^2H$-depleted hydrogen is incorporated into phytol and its precursors during the step-wise hydrogenation catalyzed by GGR ($\varepsilon_{GGR} \cong$ –650 ‰; Chikaraishi et al., 2009). The $\varepsilon_{L/W}$ values of phytol (and its dehydration product phytadiene) investigated in a wide range of eukaryotes so far are all significantly large and negative (e.g., –357 to –278 ‰ for phytol in dinoflagellate, coccolithophore, marsh grass, cucumber, and conifer; Fig. 7A).

The hydrogenation step catalyzed by GGR is of particular interest to this study, as it is also the last step of lipid biosynthesis shared among all tetraether-producing archaea (Step 9; Fig. S1). We propose double bond saturation catalyzed by GGR as the likely source of additional $^2H$ depletion in archaeal isoprenoid lipids. In fact, results of the isotope flux-balance model for *N. maritimus* also indicated that the GGR reduction step is strongly fractionating ($\varepsilon_{GGR}$ = –690 to –820 ‰ if $\varepsilon_{NADPH}$ = –100 to –300 ‰, depending on the degree of water exchange equivalent to $x_{ex}$ in this study), regardless of how other model parameters are set (Leavitt et al., 2023). Thus, the double bond reduction catalyzed by GGR could impart such a large isotope effect on 8 out of 80 or 10 % of H's per biphytane molecule (Fig. S1), similar to the process demonstrated for the step-wise reduction by GGR in phytol biosynthesis (Chikaraishi et al., 2009).

Altogether, the isotope flux-balance model for *A. fulgidus* allows us to put reasonable constraints on the direction and magnitude of isotope fractionation associated with a specific subset of H fluxes under our experimental conditions (e.g., $\varepsilon_{W,indirect}$ = –599 to –436 ‰ at $s$ = 0 %; –519 to –276 ‰ at $s$ = 100 % when $\varepsilon_{W,direct}$ = –100 ‰; Fig. 5A), which subsequently informs specific biochemical steps to investigate for further mechanistic understanding. Comparison with eukaryotic lipids, which are produced by entirely different organisms but share certain core biochemical steps during lipid synthesis, elucidates two processes that are likely responseible for consistently large and negative $\varepsilon_{L/W}$ values in both eukaryotic and archaeal lipids. These include upstream isomerization steps involving five-carbon units (part of the $f_{W,direct}$ flux in our model) and downstream reduction step catalyzed by GGR (part of the $f_{W,indirect}$ flux in our model) that imparts additional $^2H$ depletion in some eukaryotic isoprenoid lipids (e.g., phytol and associated products) and archaeal tetraethers.

#### 5.3.2. Energy limitation and lipid-water fractionation in Archaeal versus Bacterial lipids

Besides the shared biochemical mechanisms underlying negative $\varepsilon_{L/W}$ in eukaryotic and archaeal isoprenoid lipids, another interesting pattern emerges from comparison of $\varepsilon_{L/W}$ across the three domains of life: a subset of bacterial fatty acids resembles archaeal isoprenoid lipids in its consistently negative $\varepsilon_{L/W}$ values (Fig. 6). For bacterial lipids, anaerobiosis and/or autotrophy appear to be associated with consistently large, negative values of $\varepsilon_{L/W}$. Examples include aerobic autotrophy (*Cupriavidus oxalaticus*, Zhang et al., 2009; *Paracoccus denitrificans*, Osburn et al., 2016), anaerobic autotrophy (*Desulfobacterium autotrophicum*, Campbell et al., 2009; *Desulfococcus multivorans*, Dawson et al., 2015; *P. denitrificans*, *Desulfobacterium autotrophicum*, *Desulfovibrio alaskensis*, Osburn et al., 2016), and anaerobic heterotrophy (*D. multivorans*, Dawson et al., 2015; *P. denitrificans*, *Escherichia coli*, *D. autotrophicum*, *Desulfobacter hydrogenophilus*, *D. alaskensis*, *Desulfolobus propionicus*, Osburn et al., 2016) (Fig. 6; Fig. 7B). Of these modes of metabolism, aerobic or anaerobic autotrophy has a more constrained range of $\varepsilon_{W/L}$ and more overlaps with $\varepsilon_{L/W}$ observed in archaeal lipids, compared to anaerobic heterotrophy (Fig. 6; Fig. 7B). We propose that NADPH flux imbalances associated with energy limitation that broadly characterize autotrophic and/or anaerobic modes of metabolism contribute to the apparent similarity in $\varepsilon_{L/W}$ observed between the domains of Bacteria and Archaea.

The concept of NADPH flux imbalance set forth by Wijker et al. (2019) provides a quantitative framework to relate metabolism-dependent patterns of $\varepsilon_{L/W}$ observed in aerobic heterotrophs to the fluxes of H through specific dehydrogenase and transhydrogenase enzymes. For the highly conserved fatty acid biosynthesis pathway, NADPH serves as the reducing agent for the reduction of acyl intermediates (Wakil et al., 1983). As a result, NADPH accounts for ~ 50 % of fatty acid H (Sessions et al., 1999). Wijker et al. (2019) showed that $\varepsilon_{L/W}$ values of fatty acids produced by five wild-type species of aerobic heterotrophic bacteria are positively correlated with relative NADPH imbalance flux. Among the tested aerobic heterotrophs, two species (*E. coli* and *B. subtilis*) had moderately negative values of NADPH flux imbalance (–32 and –11 %, respectively) (Wijker et al., 2019). Here, negative values reflect underproduction of NADPH where catabolic production of NADPH does not meet the anabolic requirement (Wijker et al., 2019). Furthermore, the results from *E. coli* knockout mutants confirmed the direction of isotope fractionation for specific transhydrogenases (e.g., $^2H$-depletion by NADPH-producing PntAB and $^2H$-enrichment by NADPH-consuming UDhA) (Wijker et al., 2019).

For microbes adapted to chronic energy limitation, even more negative values of NADPH flux imbalance would be expected where just enough NADPH is produced such that most to all of it is used for biosynthesis (i.e., little to no flux from NADPH back to NADH). This prediction is consistent with the general concept of energy spilling (also known as growth uncoupling or overflow metabolism), which suggests that microbes under energy limitation tend to have more efficient biomass production (Russell, 2007). For example, *E. coli* grown aerobically resulted in more than 9-fold increase in ATP production per mole of glucose compared to the anaerobic counterpart; however, the biomass yield was only 2-fold greater during aerobic respiration (Stouthamer and Bettenhaussen, 1977; Gottschalk, 1986). Similar phenomenon of energy spilling has also been observed in methanogenic archaea. For example, *Methanothermobacter thermautotrophicus* and *Methanococcus maripaludis* produced less biomass per mole of methane when $H_2$ (electron donor) was present in excess compared to $H_2$-limiting condition (Morgan et al., 1997; De Poorter et al., 2007; Costa et al., 2013).

In line with the observed and expected outcomes of energy limitation (negative NADPH flux imbalance and tighter coupling between catabolism and anabolism), Leavitt et al. (2023) found that $\varepsilon_{L/W}$ values for *N. maritimus* fall within the 95 % confidence interval for the extension of Wijker et al. (2019) regression when an extremely negative value (–100 %) of NADPH flux imbalance was assigned. The apparent fit of *N. maritimus* $\varepsilon_{L/W}$ on the negative end of the framework is reasonable, given that *N. maritimus* is an obligate autotroph adapted to oligotrophic nitrification with energy-efficient $CO_2$ fixation pathway (Martens-Habbena et al., 2009; Könneke et al., 2014). The fact that all archaeal lipids investigated for $\varepsilon_{L/W}$ so far fall within a relatively narrow range of negative values (Fig. 6; Fig. 7B) may, at least partially, reflect the general concept that Archaea are optimized for chronic energy limitation (Valentine, 2007). The results from this study show that, while metabolic modes and growth rates have significant impacts on $\varepsilon_{L/W}$ within a single organism (*A. fulgidus*), the observed variation in $\varepsilon_{L/W}$ still falls within the overall range observed across archaeal lipids (e.g., heterotrophic and autotrophic *A. fulgidus* 'Af' data *vs.* other archaeal lipids data; Fig. 7B).

The similarity between archaeal lipids and a subset of anaerobic and/or autotrophic bacterial lipids is striking (Fig. 6; Fig. 7B) given the fundamental differences in fatty acid and isoprenoid lipid biosynthesis pathways. This suggests that factors controlling microbial $\varepsilon_{L/W}$ may not be domain-specific; instead, common challenges associated with anaerobic respiration and/or autotrophy (i.e., lower free energy yields and/or additional energetic costs for $CO_2$ fixation) may become primary controlling factors of $\varepsilon_{L/W}$ for both Bacteria and Archaea. Notably, the range of $\varepsilon_{L/W}$ in fatty acids produced by sulfate-reducing bacteria (SRB) is much narrower compared to that observed in aerobic heterotrophs regardless of metabolic pathway or substrate (Fig. 7B). In other words, while archaeal isoprenoid lipids and bacterial fatty acids differ in fundamental biochemical mechanism, it may be possible that external

factors such as energy limitation cause an apparent convergence of $\varepsilon_{L/W}$ values among prokaryotic lipids found in certain environments.

One of the transhydrogenases that plays an important role in SRB is NfnAB, and it has been shown that this enzyme is important for H isotope fractionation in *D. alaskensis* (Leavitt et al., 2016). The details of the magnitude of $\varepsilon_{L/W}$ set by NfnAB under severe NADPH underproduction may be complicated by other processes such as intracellular isotope distillation (i.e., more quantitative transfer of NADPH hydride to lipids) as suggested by Leavitt et al. (2016). Regardless, given that decoupling of NADPH production for anabolism from NADH for catabolism becomes more important during energy limitation, transhydrogenases that are widely distributed among anaerobic bacteria (namely NfnAB; Pereira et al., 2011; Leavitt et al., 2016; Buckel and Thauer, 2018) may be key contributing factors for the negative $\varepsilon_{W/L}$ observed across these organisms (Fig. 6; Fig. 7B). It is worth noting that *nfnAB* was not found in archaeal species investigated by Pereira et al. (2011), including *A. fulgidus*.

A complex interplay among environmental, physiological, and enzymatic factors underlies net isotope fractionation patterns observed in a biosynthetic product such as $\varepsilon_{L/W}$. For archaeal lipids and a subset of bacterial lipids, however, two factors appear to play key roles in shaping the consistently negative $\varepsilon_{L/W}$ patterns observed in the lipids from both domains: highly fractionating enzymatic steps (e.g., GGR in archaeal isoprenoid lipid biosynthesis; transhydrogenases in bacterial fatty acid biosynthesis) and energy limitation (i.e., NADPH flux imbalance). The negative $\varepsilon_{L/W}$ commonly observed in archaea and a subset of bacteria is likely a convergent feature resulting from a combination of both factors. A better mechanistic understanding of factors conducive to similar patterns of $\varepsilon_{L/W}$ in bacterial and archaeal lipids could lead to biogeochemical and/or ecological insights that are unique to microbial life. This would, in turn, significantly expand the application of lipid biomarkers as paleoenvironmental or paleoecological proxy currently possible with eukaryotic or bacterial lipids alone.

## 6. Conclusion

In this study, we conducted water isotope label experiments with a metabolically flexible and well-studied model archaeon *A. fulgidus* and quantified the hydrogen isotope fractionation between lipids and water in response to different carbon substrates and electron donor–acceptor pairs. We observed changes in regression parameters among experimental conditions, where higher slopes ($f_W \cdot {}^2\alpha_{L/W}$) were observed in autotrophic compared to heterotrophic conditions and during stationary compared to exponential growth phase. The bio-isotopic model further constrains individual parameters such as fluxes that reflect water isotope composition (i.e., not affected by substrate isotope composition) ($f_W$) and isotope fractionation between lipids and water ($\varepsilon_{L/W}$) that together make up the slope. These results are consistent with observations from regression parameters, where $f_W$ is larger under autotrophic condition and during stationary growth phase compared to the heterotrophic conditions and exponential growth phase. The model results also allow us to constrain plausible ranges of isotope fractionation associated with a specific route of hydrogen flux (e.g., flux for direct water incorporation *vs*. flux from water through cofactors). Based on the model results, two main mechanisms of observed $^2$H depletion in *A. fulgidus* tetraether lipids: 1) isotopic re-equilibration of $C_5$ units during isomerization steps, as part of the $f_{W,direct}$ flux; and 2) large isotope fractionation associated with the last reduction step catalysed by GGR, as part of the $f_{W,indirect}$ flux. These proposed mechanisms are also consistent with observations across $^2$H-depleted eukaryotic lipids, including those with particularly negative $\varepsilon_{L/W}$ values (e.g., phytol), and archaeal lipids reported in previous studies. Furthermore, the shared negative $\varepsilon_{L/W}$ values between fatty acids in anaerobic and/or autotrophic bacteria and isoprenoids in archaea may be associated with the general state of energy limitation experienced by the different groups of organisms. Additional experimental work with archaea that use carbon metabolism pathways that have not been examined with the bio-isotopic model (i.e., 3HP/4HB and reductive Wood-Ljungdahl pathways) as well as more systematic comparisons between bacterial and archaeal lipids will help determine the scope of applicability for microbial lipid $\varepsilon_{L/W}$ in paleoenvironmental and paleoecological studies.

## CRediT authorship contribution statement

**Jeemin H. Rhim:** Writing – review & editing, Writing – original draft, Visualization, Methodology, Investigation, Data curation, Conceptualization. **Sebastian Kopf:** Writing – review & editing, Supervision, Resources, Methodology, Funding acquisition, Formal analysis, Conceptualization. **Jamie McFarlin:** Writing – review & editing, Investigation. **Ashley E. Maloney:** Writing – review & editing, Investigation. **Harpreet Batther:** Writing – review & editing, Investigation. **Carolynn M. Harris:** Writing – review & editing, Investigation. **Alice Zhou:** Writing – review & editing, Investigation. **Xiahong Feng:** Writing – review & editing, Investigation. **Yuki Weber:** Writing – review & editing, Investigation. **Shelley Hoeft-McCann:** Writing – review & editing, Investigation. **Ann Pearson:** Writing – review & editing, Supervision, Resources, Funding acquisition. **William D. Leavitt:** Writing – review & editing, Supervision, Resources, Funding acquisition, Conceptualization.

## Data availability

Access to all data products and code for the isotope flux-balance model for this manuscript are available through the Open Science Framework at https://doi.org/10.17605/OSF.IO/UD82X.

## Declaration of competing interest

The authors declare that they have no known competing financial interests or personal relationships that could have appeared to influence the work reported in this paper.

## Acknowledgements

This research was supported by funding from: collaborative research grant NSF EAR #1928303 (WDL, SHK); the American Chemical Society PRF #57209-DNI2 (WDL, YW); Simons Foundation Award #623881 (WDL); Swiss National Science Foundation P2BSP2_168716 (YW); NSF OCE-1843285 and 1702262 (AP). JHR was supported by the Dartmouth College Society of Fellows. We thank Ashley Maloney (CU Boulder), Felix Elling (then at Harvard), and Beverly Chiu (then at Dartmouth) for expert laboratory assistance. We acknowledge the analytical contributions of the CU Boulder Earth Systems Stable Isotope Lab (CUBES-SIL) Core Facility (RRID:SCR_019300).

## Appendix A. Supplementary material

These include the Measurement of lactate hydrogen isotopic composition; Overview of hydrogen budget; Culturing conditions for Acidianus sp. and Metallosphaera sedula; Full list of references for Figure 7; and Supplemental Figures 1–2. Figure S1 (Overview of hydrogen sources for tetraether biosynthesis in Archaeoglobus fulgidus); and Figure S2 (Isotope flux-balance model results for Archaeoglobus fulgidus). Supplementary material to this article can be found online at https://doi.org/10.1016/j.gca.2024.09.032.

## References

Achenbach-Richter, L., Stetter, K.O., Woese, C.R., 1987. A possible biochemical missing link among archaebacteria. Nature 327, 348–349.

Andersen, N., Paul, H.A., Bernasconi, S.M., McKenzie, J.A., Behrens, A., Schaeffer, P., Albrecht, P., 2001. Large and rapid climate variability during the Messinian salinity

crisis: Evidence from deuterium concentrations of individual biomarkers. Geology 29, 799.
Bloch, K., 1959. Biogenesis and transformations of squalene. Biosynthesis of Terpenes and Sterols. Brown and Company, Little.
Brock, T.D., Brock, K.M., Belly, R.T., Weiss, R.L., 1972. Sulfolobus: A new genus of sulfur-oxidizing bacteria living at low pH and high temperature. Arch. Mikrobiol. 84, 54–68.
Buckel, W., Thauer, R.K., 2018. Flavin-based electron bifurcation, ferredoxin, flavodoxin, and anaerobic respiration with protons (Ech) or NAD$^+$ (Rnf) as electron acceptors: a historical review. Front. Microbiol. 9, 401.
Campbell, B.J., Li, C., Sessions, A.L., Valentine, D.L., 2009. Hydrogen isotopic fractionation in lipid biosynthesis by $H_2$-consuming *Desulfobacterium autotrophicum*. Geochim. Cosmochim. Acta 73, 2744–2757.
Chikaraishi, Y., Naraoka, H., 2003. Compound-specific δD–$\delta^{13}$C analyses of *n*-alkanes extracted from terrestrial and aquatic plants. Phytochemistry 63, 361–371.
Chikaraishi, Y., Naraoka, H., Poulson, S.R., 2004. Carbon and hydrogen isotopic fractionation during lipid biosynthesis in a higher plant (*Cryptomeria japonica*). Phytochemistry 65, 323–330.
Chikaraishi, Y., Tanaka, R., Tanaka, A., Ohkouchi, N., 2009. Fractionation of hydrogen isotopes during phytol biosynthesis. Org. Geochem. 40, 569–573.
Costa, K.C., Yoon, S.H., Pan, M., Burn, J.A., Baliga, N.S., Leigh, J.A., 2013. Effects of $H_2$ and formate on growth yield and regulation of methanogenesis in *Methanococcus maripaludis*. J. Bacteriol. 195, 1456–1462.
Dawson, K.S., Osburn, M.R., Sessions, A.L., Orphan, V.J., 2015. Metabolic associations with archaea drive shifts in hydrogen isotope fractionation in sulfate-reducing bacterial lipids in cocultures and methane seeps. Geobiology 13, 462–477.
De Poorter, L.M.I., Geerts, W.J., Keltjens, J.T., 2007. Coupling of *methanothermobacter thermautotrophicus* methane formation and growth in fed-batch and continuous cultures under different $H_2$ gassing regimens. Appl. Environ. Microbiol. 73, 740–749.
Dirghangi, S.S., Pagani, M., 2013. Hydrogen isotope fractionation during lipid biosynthesis by *Haloarcula marismortui*. Geochim. Cosmochim. Acta 119, 381–390.
Disch, A., Schwender, J., Müller, C., Lichtenthaler, H.K., Rohmer, M., 1998. Distribution of the mevalonate and glyceraldehyde phosphate/pyruvate pathways for isoprenoid biosynthesis in unicellular algae and the cyanobacterium *Synechocystis* PCC 6714. Biochem. J. 333, 381–388.
Estep, M.F., Hoering, T.C., 1980. Biogeochemistry of the stable hydrogen isotopes. Geochim. Cosmochim. Acta 44, 1197–1206.
Gottschalk (1986) Regulation of Bacterial Metabolism. In: Bacterial Metabolism. Springer Series in Microbiology. Springer. https://doi.org/10.1007/978-1-4612-1072-6_7.
Hayes, J.M., 2001. Fractionation of the isotopes of carbon and hydrogen in biosynthetic processes. Rev. Mineral. Geochem. 43 (1), 225–277.
Hendrickson, E.L., Leigh, J.A., 2008. Roles of coenzyme $F_{420}$ -reducing hydrogenases and hydrogen- and $F_{420}$ -dependent methylenetetrahydromethanopterin dehydrogenases in reduction of $f_{420}$ and production of hydrogen during methanogenesis. J. Bacteriol. 190, 4818–4821.
Hocking, W.P., Stokke, R., Roalkvam, I., Steen, I.H., 2014. Identification of key components in the energy metabolism of the hyperthermophilic sulfate-reducing archaeon *Archaeoglobus fulgidus* by transcriptome analyses. Front. Microbiol. 5, 95.
Jain, S., Caforio, A., Driessen, J.M., 2014. Biosynthesis of archaeal membrane ether lipids. Front. Microbiol. 5, 641.
Kaneko, M., Kitajima, F., Naraoka, H., 2011. Stable hydrogen isotope measurement of archaeal ether-bound hydrocarbons. Org. Geochem. 42, 166–172.
Könneke, M., Schubert, D.M., Brown, P.C., Hügler, M., Standfest, S., Schwander, T., Schada Von Borzyskowski, L., Erb, T.J., Stahl, D.A., Berg, I.A., 2014. Ammonia-oxidizing archaea use the most energy-efficient aerobic pathway for $CO_2$ fixation. Proc. Natl. Acad. Sci. 111, 8239–8244.
Kopec, B.G., Feng, X., Posmentier, E.S., Sonder, L.J., 2019. Seasonal deuterium excess variations of precipitation at summit, greenland, and their climatological significance. J. Geophys. Res. Atmospheres 124, 72–91.
Kopf, S., Davidheiser-Kroll, B., Kocken, I., 2021. Isoreader: An R package to read stable isotope data files for reproducible research. J. Open Source Softw. 6, 2878.
Kunow, J., Schwörer, B., Stetter, K.O., Thauer, R.K., 1993. A $F_{420}$-dependent NADP reductase in the extremely thermophilie sulfate-reducing *Archaeoglobus fulgidus*. Arch. Microbiol. 160, 199–205.
Ladd, S.N., Sachs, J.P., 2017. $^2H/^1H$ fractionation in lipids of the mangrove *Bruguiera gymnorhiza* increases with salinity in marine lakes of Palau. Geochim. Cosmochim. Acta 204, 300–312.
Lai, D., Springstead, J.R., Monbouquette, H.G., 2008. Effect of growth temperature on ether lipid biochemistry in *Archaeoglobus fulgidus*. Extremophiles 12, 271–278.
Leavitt W. D., Venceslau S. S., Pereira I. A. C., Johnston D. T. and Bradley A. S. (2016) Fractionation of sulfur and hydrogen isotopes in *Desulfovibrio vulgaris* with perturbed DsrC expression ed. R. Boden. *FEMS Microbiol. Lett.* **363**, fnw226.
Leavitt, W.D., Kopf, S.H., Weber, Y., Chiu, B., McFarlin, J.M., Elling, F.J., Hoeft-McCann, S., Pearson, A., 2023. Controls on the hydrogen isotope composition of tetraether lipids in an autotrophic ammonia-oxidizing marine archaeon. Geochim. Cosmochim. Acta 352, 194–210.
Lengger, S.K., Weber, Y., Taylor, K.W.R., Kopf, S.H., Berstan, R., Bull, I.D., Mayser, J., Leavitt, W.D., Blewett, J., Pearson, A., Pancost, R.D., 2021. Determination of the $\delta^2H$ values of high molecular weight lipids by high-temperature gas chromatography coupled to isotope ratio mass spectrometry. Rapid Commun. Mass Spectrom. 35, e8983.
Lichtenthaler, H.K., 1999. The 1-Deoxy-D-Xylulose-5-phosphate pathway of isoprenoid biosynthesis in plants. Annu. Rev. Plant Physiol. Plant Mol. Biol. 50, 47–65.
Lichtenthaler, H.K., Rohmer, M., Schwender, J., 1997. Two independent biochemical pathways for isopentenyl diphosphate and isoprenoid biosynthesis in higher plants. Physiol. Plant. 101, 643–652.
Lynen, F., Eggerer, H., Henning, U., Kessel, I., 1958. Farnesyl-pyrophosphat und 3-Methyl-$\Delta^3$-butenyl-1-pyrophosphat, die biologischen Vorstufen des Squalens. Zur Biosynthese der Terpene. III. *Angew. Chem.* 70, 738–742.
Maloney, A.E., Shinneman, A.L.C., Hemeon, K., Sachs, J.P., 2016. Exploring lipid $^2H/^1H$ fractionation mechanisms in response to salinity with continuous cultures of the diatom *Thalassiosira pseudonana*. Org. Geochem. 101, 154–165.
Martens-Habbena, W., Berube, P.M., Urakawa, H., De La Torre, J.R., Stahl, D.A., 2009. Ammonia oxidation kinetics determine niche separation of nitrifying Archaea and Bacteria. Nature 461, 976–979.
McFarlin, J.M., Axford, Y., Masterson, A.L., Osburn, M.R., 2019. Calibration of modern sedimentary $\delta^2H$ plant wax-water relationships in Greenland lakes. Quat. Sci. Rev. 225, 105978.
Möller-Zinkhan, D., Börner, G., Thauer, R.K., 1989. Function of methanofuran, tetrahydromethanopterin, and coenzyme $F_{420}$ in *Archaeoglobus fulgidus*. Arch. Microbiol. 152, 362–368.
Möller-Zinkhan, D., Thauer, R.K., 1990. Anaerobic lactate oxidation to 3 $CO_2$ by *Archaeoglobus fulgidus* via the carbon monoxide dehydrogenase pathway: demonstration of the acetyl-CoA carbon-carbon cleavage reaction in cell extracts. Arch. Microbiol. 153, 215–218.
Morgan, R.M., Pihl, T.D., Lling, J.R.N., Reeve, J.N., 1997. Hydrogen regulation of growth, growth yields, and methane gene transcription in *Methanobacterium thermoautotrophicum* ΔH. J. Bacteriol. 179 (3), 889–898.
Osburn, M.R., Dawson, K.S., Fogel, M.L., Sessions, A.L., 2016. Fractionation of hydrogen isotopes by sulfate- and nitrate-reducing bacteria. Front. Microbiol. 7, 1166.
Pearson, A., 2014. Lipidomics for geochemistry. In: Treatise on Geochemistry. Elsevier, pp. 291–336.
Pereira, I.A.C., Ramos, A.R., Grein, F., Marques, M.C., Da Silva, S.M., Venceslau, S.S., 2011. A comparative genomic analysis of energy metabolism in sulfate reducing bacteria and archaea. Front. Microbiol. 2, 69.
Reed, D.W., Hartzell, P.L., 1999. The *Archaeoglobus fulgidus* D-lactate dehydrogenase Is a $Zn^{2+}$ flavoprotein. J. Bacteriol. 181 (24), 7580–7587.
Rhim, J.H., Zhou, A., Amenabar, M.J., Boyer, G.M., Elling, F.J., Weber, Y., Pearson, A., Boyd, E.S., Leavitt, W.D., 2024. Mode of carbon and energy metabolism shifts lipid composition in the thermoacidophile *Acidianus*. Appl. Environ. Microbiol.
Rohmer, M., Knani, M., Simonin, P., Sutter, B., Sahm, H., 1993. Isoprenoid biosynthesis in bacteria: a novel pathway for the early steps leading to isopentenyl diphosphate. Biochem. J. 295, 517–524.
Russell, J.B., 2007. The energy spilling reactions of bacteria and other organisms. Microb. Physiol. 13, 1–11.
Sachs, J.P., 2014. Hydrogen Isotope Signatures in the Lipids of Phytoplankton. In *Treatise on Geochemistry*. Elsevier. 12, 79–94.
Sachs, J.P., Kawka, O.E., 2015. The Influence of Growth Rate on $^2H/^1H$ Fractionation in Continuous Cultures of the Coccolithophorid *Emiliania huxleyi* and the Diatom *Thalassiosira pseudonana*. PLoS One 10, e0141643.
Sachs, J.P., Maloney, A.E., Gregersen, J., Paschall, C., 2016. Effect of salinity on $^2H/^1H$ fractionation in lipids from continuous cultures of the coccolithophorid *Emiliania huxleyi*. Geochim. Cosmochim. Acta 189, 96–109.
Sachs, J.P., Maloney, A.E., Gregersen, J., 2017. Effect of light on $^2H/^1H$ fractionation in lipids from continuous cultures of the diatom *Thalassiosira pseudonana*. Geochim. Cosmochim. Acta 209, 204–215.
Sachse, D., Billault, I., Bowen, G.J., Chikaraishi, Y., Dawson, T.E., Feakins, S.J., Freeman, K.H., Magill, C.R., McInerney, F.A., van der Meer, M.T.J., Polissar, P., Robins, R.J., Sachs, J.P., Schmidt, H.-L., Sessions, A.L., White, J.W.C., West, J.B., Kahmen, A., 2012. Molecular paleohydrology: interpreting the hydrogen-isotopic composition of lipid biomarkers from photosynthesizing organisms. Annu. Rev. Earth Planet. Sci. 40, 221–249.
Sessions, A.L., 2016. Factors controlling the deuterium contents of sedimentary hydrocarbons. Org. Geochem. 96, 43–64.
Sessions, A.L., Burgoyne, T.W., Schimmelmann, A., Hayes, J.M., 1999. Fractionation of hydrogen isotopes in lipid biosynthesis. Org. Geochem. 30, 1193–1200.
Sessions, A.L., Jahnke, L.L., Schimmelmann, A., Hayes, J.M., 2002. Hydrogen isotope fractionation in lipids of the methane-oxidizing bacterium *Methylococcus capsulatus*. Geochim. Cosmochim. Acta 66, 3955–3969.
Sessions, A.L., Sylva, S.P., Summons, R.E., Hayes, J.M., 2004. Isotopic exchange of carbon-bound hydrogen over geologic timescales. Geochim. Cosmochim. Acta 68, 1545–1559.
Shima, S., Pilak, O., Vogt, S., Schick, M., Stagni, M.S., Meyer-Klaucke, W., Warkentin, E., Thauer, R.K., Ermler, U., 2008. The crystal structure of [Fe]-hydrogenase reveals the geometry of the active site. Science 321, 572–575.
Steinsbu, B.O., Thorseth, I.H., Nakagawa, S., Inagaki, F., Lever, M.A., Engelen, B., Ovreas, L., Pedersen, R.B., 2010. *Archaeoglobus sulfaticallidus* sp. nov., a thermophilic and facultatively lithoautotrophic sulfate-reducer isolated from black rust exposed to hot ridge flank crustal fluids. Int. J. Syst. Evol. Microbiol. 60, 2745–2752.
Stouthamer, A.H., Bettenhaussen, C.W., 1977. A continuous culture study of an ATPase-negative mutant of *Escherichia coli*. Arch. Microbiol. 113, 185–189.
Thauer, R.K., 2012. The wolfe cycle comes full circle. Proc. Natl. Acad. Sci. 109, 15084–15085.

Valentine, D.L., 2007. Adaptations to energy stress dictate the ecology and evolution of the Archaea. Nat. Rev. Microbiol. 5, 316–323.

Valentine, D.L., Sessions, A.L., Tyler, S.C., Chidthaisong, A., 2004. Hydrogen isotope fractionation during $H_2/CO_2$ acetogenesis: hydrogen utilization efficiency and the origin of lipid-bound hydrogen. Geobiology 2, 179–188.

Van Der Meer, M.T.J., Benthien, A., French, K.L., Epping, E., Zondervan, I., Reichart, G.-J., Bijma, J., Sinninghe Damsté, J.S., Schouten, S., 2015. Large effect of irradiance on hydrogen isotope fractionation of alkenones in *Emiliania huxleyi*. Geochim. Cosmochim. Acta 160, 16–24.

Von Bünau, R., Zirngibl, C., Thauer, R.K., Klein, A., 1991. Hydrogen-forming and coenzyme-$F_{420}$ -reducing methylene tetrahydromethanopterin dehydrogenase are genetically distinct enzymes in *Methanobacterium thermoautotrophicum* (Marburg). Eur. J. Biochem. 202, 1205–1208.

Wakil, S.J., Stoops, J.K., Joshi, V.C., 1983. Fatty acid synthesis and its regulation. Ann. Rev. Biochem. 52, 537–579.

Wijker, R.S., Sessions, A.L., Fuhrer, T., Phan, M., 2019. $^2H/^1H$ variation in microbial lipids is controlled by NADPH metabolism. Proc. Natl. Acad. Sci. 116, 12173–12182.

Wolfshorndl, M., Danford, R., Sachs, J.P., 2019. $^2H/^1H$ fractionation in microalgal lipids from the North Pacific Ocean: Growth rate and irradiance effects. Geochim. Cosmochim. Acta 246, 317–338.

Wu, W., Meador, T.B., Könneke, M., Elvert, M., Wegener, G., Hinrichs, K., 2020. Substrate-dependent incorporation of carbon and hydrogen for lipid biosynthesis by *Methanosarcina barkeri*. Environ. Microbiol. Rep. 12, 555–567.

Zhang, X., Gillespie, A.L., Sessions, A.L., 2009. Large D/H variations in bacterial lipids reflect central metabolic pathways. Proc. Natl. Acad. Sci. 106, 12580–12586.

Zhang, Z., Sachs, J.P., 2007. Hydrogen isotope fractionation in freshwater algae: I. Variations among lipids and species. Org. Geochem. 38, 582–608.

Zirngibl, C., Hedderich, R., Thauer, R.K., 1990. $N^5$, $^{N1}$0-Methylenetetrahydromethanopterin dehydrogenase from *Methanobacterium thermoautotrophicu*m has hydrogenase activity. FEBS Lett. 261, 112–116.